# FINAL PUBLISHABLE REPORT

| | |
|---|---|
| Grant Agreement number | 17IND04 EMPRESS 2 |
| Project short name: | EMPRESS 2 |
| Project full title: | Enhancing process efficiency through improved temperature measurement 2 |

| | | |
|---|---|---|
| Project start date and duration: | 1 May 2018, 42 months | |
| Coordinator: Jonathan Pearce, NPL Tel: +44 20 8943 6886 E-mail: jonathan.pearce@npl.co.uk<br>Project website address:<br>https://www.strath.ac.uk/research/advancedformingresearchcentre/whatwedo/collaborativeprojects/empress2project/ | | |
| Internal Funded Partners:<br>1. NPL, United Kingdom<br>2. CEM, Spain<br>3. CMI, Czech Republic<br>4. DTI, Denmark<br>5. DTU, Denmark<br>6. INRIM, Italy<br>7. JV, Norway<br>8. PTB, Germany<br>9. TUBITAK, Turkey<br>10. UL, Slovenia | External Funded Partners:<br>11. CNR, Italy<br>12. Elkem, Norway<br>13. IPHT, Germany<br>14. ITT, Italy<br>15. MUT, Germany<br>16. STRATH, United Kingdom<br>17. UC3M, Spain<br>18. UCAM, United Kingdom<br>19. UoS, United Kingdom | Unfunded Partners:<br>20. ACERINOX, Spain<br>21. B&W Volund, Denmark<br>22. BAE, United Kingdom<br>23. CCPI, United Kingdom<br>24. JM, United Kingdom<br>25. Sensia, Spain |
| RMG: - | | |

**TABLE OF CONTENTS**

# 1 Overview

The overall aim of the project was to enhance the efficiency of high value manufacturing processes by improving temperature measurement and control capabilities. Enhanced efficiency includes improved energy efficiency (and hence reduced emissions); improved product consistency (and hence reduced waste); increased sensor stability, reliability and longevity (and hence reduced operator intervention). All of the activities in the project were characterised by the implementation of traceability to the International Temperature Scale of 1990 (ITS-90) in-process. Such traceability is critical to establishing low measurement uncertainty, e.g. < 3 °C, and reproducible process control. The main developments were the extension of traceable phosphor thermometry to 750 °C and 2D imaging, and combination with thermal IR imaging to overcome the problem of emissivity and background reflections; impartial determination of the stability of dual-walled mineral insulated, metal-sheathed thermocouples compared with conventional ones, and characterisation of a reference function for new Pt-40%Rh/Pt-6%Rh thermocouples; use of a portable standard flame to enable creation of inexpensive flame imaging apparatus, and in-process reduction of uncertainty in temperature control of waste incineration; development of several types of fibre-optic thermometer for various applications in harsh environments which are not amenable to other more conventional temperature sensors. These outputs have been extensively demonstrated in industrial processes throughout Europe.

# 2 Need

High value manufacturing depends on accurate, traceable temperature measurement. This project sought to address four contemporary thermometry challenges in high value manufacturing (each of which relates to one of the project's technical objectives).

1. Below 750 °C many industrial processes require reliable surface thermometry e.g. welding, coating, forging and forming. Conventional non-contact surface thermometry techniques by thermal imaging/single spot radiometry were prone to large errors (generally tens of degrees) due to reflected thermal radiation and unknown emissivity. Surface contact thermometry approaches were also prone to equally large errors. New traceable approaches were needed.
2. Above 1200 °C sensor drift was a significant unaddressed issue for e.g. casting, forging and heat treatment, causing errors of tens and sometimes hundreds of degrees. There was therefore a need for more stable sensors and for the standardisation of at least one new thermocouple type to fill the gap between 1200 °C and 1800 °C.
3. The measurement of combustion temperature was extremely challenging for many reasons. For example, a contact probe (e.g. a thermocouple) will not reach thermal equilibrium with the flame because it radiates heat away faster than the flame can supply it, resulting in an under-reading of the temperature by hundreds of degrees. Non-contact thermometry was fraught with difficulties such as the three-dimensional nature of the flame and its strong spatial temperature variation. For this reason many users have resorted to complex and exotic laser-based systems to probe the combustion species directly with a wide range of different techniques. Traceability was almost non-existent; for example, thermocouple measurements of flame temperatures can be in error by hundreds of degrees. A verified 'standard flame' (such as that developed during EMPIR JRP 14IND04 EMPRESS, hereafter known as EMPRESS) that can be transported to users' sites was needed, as well as case studies to demonstrate its utility.
4. Many processes were not amenable to any conventional thermometry techniques due to e.g. inaccessibility, ionising radiation, electromagnetic interference, and contamination; here methods based on optical fibres were ideal, but there were no traceable calibration techniques, and in some cases (ionising radiation) the darkening of the fibre needs to be overcome by the development of practical 'hollow core' fibres.

By introducing traceability to ITS-90 directly into the process and through developing novel calibration techniques, as well as sensors with immunity to perturbing influences, the uncertainty of thermometry in various areas of industry has been substantially reduced from the current state of the art measurements, with a corresponding enhancement in the efficiency of the process. This project addressed the four contemporary thermometry challenges where the need for improvement was greatest: namely surface contact temperature probes, thermocouples, combustion thermometry, and optical fibres.

# 3 Objectives

The overall goal of the project was to enhance the efficiency of high value manufacturing processes by improving temperature measurement and control capabilities.

The specific objectives of the project were to:

1. **Implement traceable surface temperature measurement in-process** – by developing accurate methods for phosphor thermometry for temperatures up to 750 °C. Such methods will also be combined with quantitative thermography in order to determine emissivity for temperature measurements over wide fields of view. The in-process target uncertainty for these techniques is less than 3 °C at 750 °C.
2. **Reduce uncertainty of temperature measurement in-process** – through developing and implementing improved and traceable low-drift temperature sensors for enhanced process efficiency and improved temperature control. This will address the traceability of optimised Pt-Rh thermocouples, and a reduction in the uncertainty of new in-process temperature sensors such as the double-walled mineral-insulated, metal sheathed (MI) thermocouples through mitigating insulation resistance breakdown and drift effects. The uncertainty will be less than 3 °C up to 1200 °C for the mineral-insulated, metal sheathed thermocouples. -
3. **Implement *in-situ* traceable combustion thermometry** – by validating an *in-situ* combustion reference standard (standard flame) of known temperature with an in-process target uncertainty of less than 0.5 %. In addition, to use the combustion reference standard to evaluate the linkage between portable standard reference flames, improved process temperature control, and an enhancement in process efficiency.
4. **Introduce traceable fibre-optic thermometry** – by developing reliable, accurate and validated methods for demonstrating the traceability of at least two different types of fibre-optic thermometry in hostile environments. In addition, to develop novel methods for fibre-optic thermometry, validated in at least one harsh environment with a target uncertainty of better than 5 °C up to 500 °C.
5. **To facilitate the take up of the technology and measurement infrastructure** developed in the project by the measurement supply chain, standard developing organisations, and end-users (e.g. petrochemical industry, nuclear power industry, cement manufacture, iron and steel manufacture, gas turbines and automotive industries, consumer electronics industry, metals industries, food and beverages industry, and healthcare).

# 4 Results

Good progress was made in the first EMPRESS project[1], particularly in the development of working prototypes of several novel thermometers including the phosphor thermometer, several new types of ultra-stable thermocouples, a portable standard flame and a suite of flame and combustion temperature diagnostic techniques, all of which are aimed at enabling traceability to the International Temperature Scale of 1990 (ITS-90)[2] in process. In particular, each of the key developments of the key developments was tested in at least one real-world setting. EMPRESS 2 builds on these developments. In this section, the results are summarised by objective. Where uncertainties are mentioned, these correspond to a coverage factor $k = 2$, corresponding to 95% coverage probability.

### 4.1 Objective 1: Implement traceable surface temperature measurement in-process

***- by developing accurate methods for phosphor thermometry for temperatures up to 750 °C. Such methods will also be combined with quantitative thermography in order to determine emissivity for temperature measurements over wide fields of view. The in-process target uncertainty for these techniques is less than 3 °C at 750 °C.***

In EMPRESS 2, there are three key types of phosphor thermometry systems to be developed, each with a specific type of application in mind:

[1] Pearce J V, Edler F, Elliott C J, Rosso L, Sutton G, Zante R, Machin G 2017, EMPRESS: A European Project to Enhance Process Control Through Improved Temperature Measurement, Int. J. Thermophys. 38, 118

[2] Preston-Thomas H 1990, The International Temperature Scale of 1990 (ITS-90), Metrologia 27 (1990) 3; erratum: Preston-Thomas H 1990, Metrologia 27 107

- A 2D intensity ratio phosphor thermometer, employing a traceably calibrated phosphor, to be combined with quantitative thermography, enabling the production of emissivity maps.
- A phosphor thermometer optimised for the coating of billets to enable both online monitoring of billet temperature over the entire piece during heat treatment, and 'offline' monitoring whereby the phosphor records the temperature during the heat treatment for subsequent determination. The latter approach is useful when the billet cannot be viewed.
- A fibre-optic system for remote interrogation of the phosphor with a specific application in automotive brake pad/disk temperature determination.

Development of a phosphor thermometer for surface thermometry to 750 °C

The aim of this task is to develop a phosphor thermometry capability up to 1000 °C and to demonstrate its performance in a number of trials. The accuracy of non-contact surface thermometry critically depends on knowledge of the surface emissivity. Additionally, background thermal radiation reflected from the surface can introduce significant measurement errors. Phosphor thermometry involves the interrogation of a thin phosphor coating (previously applied to the surface) following excitation from UV radiation. By measuring either the decay in the subsequent fluorescence with time or measuring the ratio of two emission bands, the temperature can be found that is independent of surface emissivity, background radiation and moderate levels of participating media between the surface and the instrument (i.e. windows, smoke etc.). By combining phosphor thermometry and established thermal imaging, it is possible to independently determine the surface emissivity and to significantly reduce thermal imaging uncertainties.

For surface thermometry for forming and forging processes, good adhesion to the metal substrate is required. This is often achieved by testing numerous ceramic binders, sintering recipes and coating processes in order to match the thermal expansion coefficient of the coating and the metal substrate over the whole temperature range to avoid delamination. Additionally, this is also affected by the environmental conditions i.e. furnace atmosphere (vacuum, gas fired or electrical furnace), and presence of graphite based lubricant during the forging process. For example, a preform or billet with a phosphor coating patch subjected to a long heat treatment inside a gas fired furnace (oxidising atmosphere with high water partial pressure) could accelerate the coating delamination due to metal surface oxidation.

NPL has successfully applied phosphor coatings to very diverse metal substrates and observed good integrity and durability of the coating for mild process conditions, and this technique is now well established. Thermal history coatings are slightly different, in that they rely on the irreversible oxidation of the rare earth element within the phosphor to indicate the highest temperature achieved. For this reason, they are either used in their amorphous sate or they need to be sintered in either a reducing atmosphere or vacuum. In order to withstand longer exposure time in harsh environments, to improve coating robustness, atmospheric plasma spray can be used to apply the phosphor powder onto the intricate component to be monitored. The measurement uncertainty in all applications described here is less than 3 °C.

To validate the in-house coatings and calibrations of the phosphor thermometry the three partners NPL, DTI and STRATH performed an intercomparison of three phosphor coatings; each partner coated one block of metal and the three samples were circulated and measured at each laboratory. The reproducibility of the temperature measurement throughout was found to be within ± 1 °C.

*Electro-thermal mechanical testing*

Soon after the start of EMPRESS 2, NPL had developed a prototype intensity ratio imaging phosphor thermometer that can measure temperatures from 20 °C to 450 °C[3]. The thermographic phosphor used was $Mg_4FGeO_6$:Mn. Typically, imaging phosphor thermometry systems make use of the intensity ratio of the phosphor emission in two discrete wavelength bands, measured simultaneously using two cameras viewing the same surface. However, difficulties can arise with image registration (the requirement to spatially align the two images) due to lens distortion, non-normal viewing angles and camera alignment, and this can result in large temperature errors. The time-domain intensity ratio technique presented here avoids these difficulties by capturing two images at different times during the phosphorescence decay process using a single monochrome camera. Each pixel of the camera integrates the light collected over the exposure time. By careful selection of an appropriate exposure time, along with the timing of each exposure (image gating), it is possible to collect two specific time integrated portions of the phosphor decay curve. The phosphor decay time can

[3] Sutton G, Greenen A, Roebuck B, Machin G 2019, Imaging phosphor thermometry from T = 20 °C to 450 °C using the time-domain intensity ratio technique, *Meas. Sci. Technol.* 30 004002

then be calculated quickly and uniquely from the ratio of these two signals and related to the temperature through calibration. With this technique, there is no requirement for high frame-rates and satisfactory results can be obtained using a relatively inexpensive camera provided that suitable triggering and exposure control are available.

This has been applied to a real-world measurement problem, namely a 3 mm x 1 mm x 20 mm steel coupon electrically heated in the NPL electro-thermal mechanical testing (ETMT) machine. Although the coupon is behind a Perspex cover, unlike thermography (thermal imaging), the phosphor thermometry is unperturbed by the cover, and, also unlike thermography, information on the emissivity is not needed. Figure 4.1.1 shows a typical 2D image of the coupon made with the new system. This offers greatly reduced uncertainty because the temperature is very difficult to measure with thermocouples (due to heat flow along the wires causing a temperature drop) and non-contact thermometry (due to unknown and temperature-dependent emissivity, and background radiation effects).

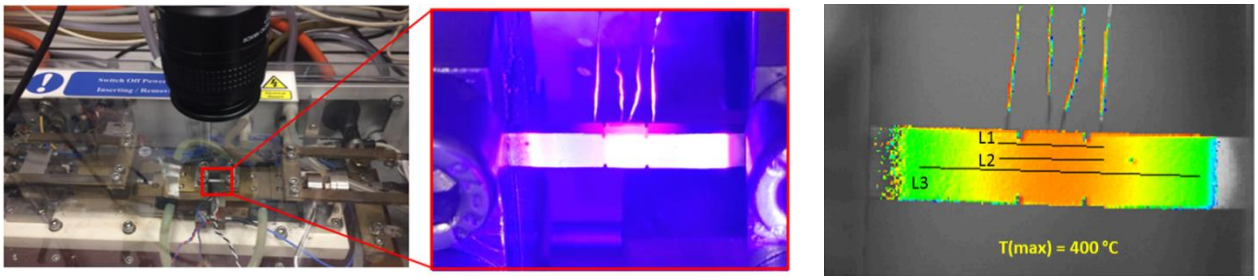


Figure 4.1.1. Phosphor thermometry applied to a coupon undergoing mechanical testing. Left: the testing apparatus, with the coupon shown in the box. Centre and right: temperature distribution (shown by colour) of the coupon.

*Photovoltaic cells*

Significant impact has been demonstrated in the application of NPL's phosphor thermometer to characterizing photovoltaic cells[4]. Accurate temperature measurements of photovoltaic (PV) devices are not always straightforward. Compromises between accuracy and spatial resolution often have to be made to give either quantitative single point measurements (e.g. thermocouples) or qualitative spatial measurements (e.g. thermal imaging). Phosphor thermometry was demonstrated in this work to measure the temperature of an encapsulated silicon photovoltaic device with an uncertainty of less than 1 °C. Comparisons with contact thermocouple probes were made under external white-light illumination and internal resistive heating. Under similar conditions, phosphor thermal imaging showed less sensitivity to sources of uncertainty such as poor probe positioning and reduced thermal contact, allowing the detection of faults and shunt induced thermal hot spots in encapsulated PV devices with a higher degree of confidence.

*Nuclear decommissioning and waste storage*

Sellafield Ltd is tasked with decommissioning the historic nuclear facilities at the Sellafield site in the UK ensuring safe and effective storage of nuclear material related to power generation (from across the UK) including spent fuel and fissile material obtained through fuel reprocessing.

Reliable surface thermometry is a key indicator over a wide spectrum of activities at the Sellafield site. For example, reliable temperatures are essential for assessing the health of nuclear material containers and is essential information for supporting the safety case of the containers. The same is the case for spent Advanced Gas Reactor (AGR) fuel which is going to be stored in ponds at the Sellafield site. This interim storage, both of spent fuel and containers is anticipated for be around 100 years until long term geological storage is available.

Reliable phosphor thermometry has been under development at NPL. Sellafield were quick to see the opportunities this approach provided for giving reliable long-term traceable temperature measurement in three key nuclear decommissioning areas; a) reliable surface thermometry of the vents of intermediate level waste containers; b) providing reliable traceable surface thermometry for the next generation storage containers for

[4] Cao Y., Koutsourakis G., Sutton G J M, et al. 2019, In situ contactless thermal characterization and imaging of encapsulated photovoltaic devices using phosphor thermometry, *Prog. Photovolt. Res. Appl.* 27 673-681

special nuclear materials (SNM) (fissile materials) (Figure 4.1.2) and c) determining reliable traceable surface temperatures for spent AGR fuel rack whilst in ponds[5].

NPL has worked with Sellafield to adapt its core metrology capability in phosphor thermometry to be suited for deployment in these situations. Work is on-going with Sellafield with a decision about deployment to be made in 2023/24.

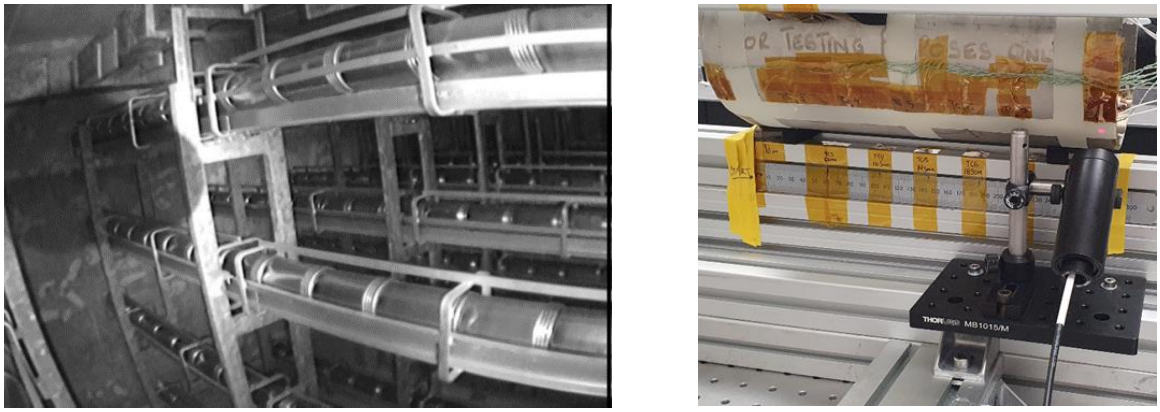

Figure 4.1.2. Left: SNM container on racks in store. Right: SNM container in laboratory at NPL undergoing phosphor thermometry tests (light vertical stripe is the phosphor on can, red spot is where thermometry is taking place).

*Marine manufacturing (welding pre- and post-heat treatment)*

Testing was performed on tube samples provided by BAE over the temperature range of interest, 22 °C to 750 °C. This is for process monitoring of the temperature before, during and after automatic robotic induction annealing for heat treatment of metal tubes (Figure 4.1.3). To verify the thermometry, a comparison of the ratio pyrometer at BAE was made with a single colour pyrometer of NPL, and MFG phosphor and thermocouples used for calibration of the phosphor. In addition, coating performance and adhesion before and after trials at both NPL and BAE was assessed and found to be satisfactory.

Trials of the NPL imaging phosphor thermometer have been successfully completed on steel pipe samples provided by BAE. The samples were phosphor coated by NPL, sent to BAE for the induction annealing process (via an automated robot), and then returned to NPL for assessment of calibration drift. Evidence of minor drift was seen, increasing with the number of heating cycles (up to 60 °C at 450 °C). It is believed that a majority of the drift is not due to the annealing process but temperature differences during the calibration process following trials, where the relationship between the phosphor and calibration (thermocouple) temperatures was not well understood. Measurements during the induction heating at BAE were not possible due to Covid-19 restrictions, and it is expected that had they been possible, the drift would be better understood.

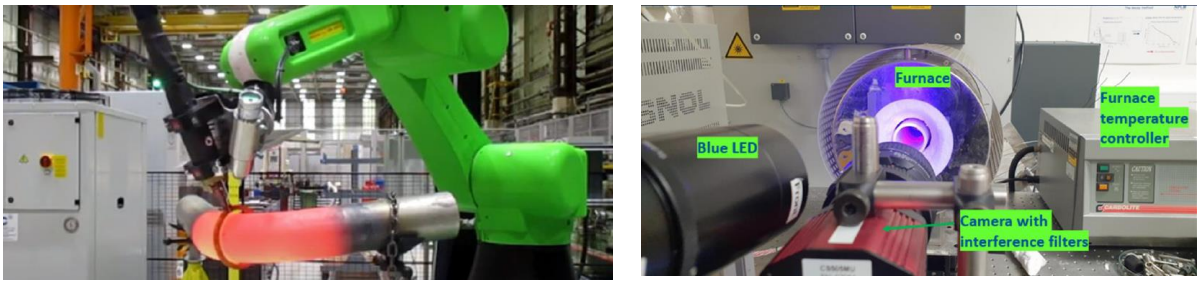


Figure 4.1.3. Left: Automatic induction annealing robot to heat treat metal tubes (image https://www.looptechnology.com/case-studies/case-study-annealing-cell-with-hand-guided-robot/). Right: Phosphor thermometry of BAE metal samples coated with MFG phosphor, performed at NPL.

[5] Sposito A, Heaps E, Sutton G, Machin G, Bernard R, Clarke S 2021, Phosphor thermometry for nuclear decommissioning and waste storage, *Nuclear Engineering and Design*, 375 (2021) 111091

Development of phosphor sensors for surface temperature monitoring on forging tools

The aim of this task is to devise a phosphor sensor that is suitable for monitoring surface temperatures on the surfaces of forging tools up to 1000 °C. Tool temperature is critical for the quality of the components produced, but it is difficult to monitor due to the extreme conditions at the tool surface (high temperature, high mechanical loads and the presence of lubricants) and intermittent access (optical access can only be gained when the press is open between operations, whilst the temperature experienced during the pressing process are the most critical). Phosphors operate at high temperatures, offer good signal to noise ratio and emissivity independent measurement, so they have the potential to meet the needs of this extreme environment. Two sensors can be envisaged: one for tool temperature monitoring on a continuous basis between every pressing operation and one for use during the setup of the apparatus, prior to actual processing, to record the surface temperature during the process when the tool is closed. The former can be achieved using an online sensor and the latter by an offline 'memory' type sensor. This task seeks to identify and characterise a suitable phosphor for each type of application.

STRATH has identified suitable phosphors with measurement capability in the relevant temperature range experienced by tools and work pieces in representative forging processes. This includes those phosphors with both on-line (i.e. live measurements) and off-line (i.e. inaccessible during the process – data is recovered afterwards) response modes. Using a selected phosphor, a coating-type sensor design has been devised for on-line surface temperature mapping, and prototypes have been manufactured. Terbium doped yttrium orthosilicate, YSO:Tb was assessed, because terbium doped phosphors have been shown to have sufficient photoluminescent intensity at temperatures above 500 °C, and exhibit decay lifetimes in millisecond timescales. A sample of 5 % terbium doped yttrium orthosilicate was produced using the sol-gel process. A measurement system based on 2D lifetime decay mapping was designed, and appropriate measurement systems and signal processing routines developed.

*Phosphor coating application and calibration for forming, forging and heat treatment*

The phosphor coatings are capable of being sprayed with thicknesses of around 35 μm while remaining durable and homogeneous. Additionally, if larger signal intensities are required the coatings can be applied thicker. Point measurements are currently achievable reliably, as the work carried out in 14IND04 EMPRESS demonstrated, although this was carried out at lower temperatures from about 20 °C to 200 °C. For the high temperature phosphor, three calibration cycles, from 20 °C to 750 °C, have been completed for the intensity ratio imaging phosphor thermometer using $Mg_4FGeO_6$:Mn phosphor and 643-2 binder. This has demonstrated a measurement uncertainty of less than 3 °C to 10 °C for temperatures below 600 °C and between 600 °C and 750 °C respectively. In addition to a high-temperature furnace system, an additional small box furnace with sapphire window has been developed and tested up to 1000 °C. This new facility provides the capability for rapid thermal cycling and *in situ* calibration of the phosphor thermometry system.

AFRC have supplied six different metal samples to NPL for testing, that would cover a very wide range of applications/sectors (specifically aerospace, oil and gas, and automotive). The materials supplied are H13 tool steel, Inconel 718+ (nickel based super alloy), C42 MOD (micro alloyed steel), Ti64 (titanium alloy) Ti-10-2-3 and Nimonic 105 (nickel-cobalt-chromium-base alloy). NPL has sent back flat square samples cut from these materials (20 mm by 20 mm) for emissivity measurement trials from 300 °C to 900 °C.

A new coating recipe supplied by a specialist coating company in the UK has solved a number of challenges associated with adhesion of the phosphor to various surfaces, with coatings remaining adhered and still retaining the previously mentioned calibration uncertainties after seven cycles between ambient temperature and about 750 °C. Some applications are described in the following.

*Heat treatment*

NPL demonstrated precision phosphor thermometry of billets during heat treatment at STRATH (AFRC). Field trials were carried out at the AFRC using the system developed by NPL on a wide range of engineering alloys including Ti64, Steel C42 MOD and Nimonic 105. The metal samples were coated on half of one side with the phosphor (MFG), and heated using an induction system up to 700 °C. The optimised phosphor coating (binder, solvent, phosphor) was employed and the optimised annealing cycle was used to minimise the risk of delamination. Samples were heated using a 15 kW Ambrell Ekoheat induction heating system in conjunction with a large inductor coil (frequency 98 kHz, skin depth about 40 mm). An additional thermal camera (LAND ARC-8-22-1000-HF) was used to measure the temperature of the bare metal and phosphor coating, to enable the emissivity to be inferred. A summary of the measurements is given in Figure 4.1.4 and its caption.

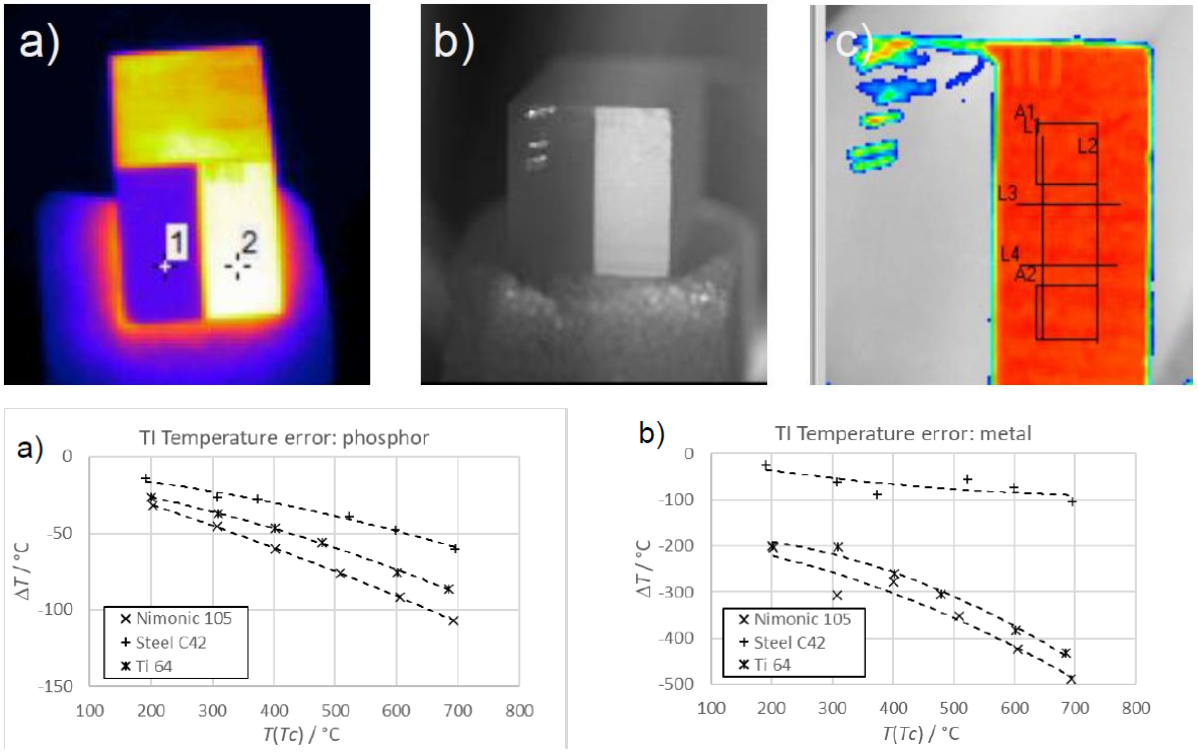


Figure 4.1.4. Top: Images taken from a) the Land thermal imager, showing the measurement locations for (1) the bare metal and (2) the phosphor coating; b) the phosphor thermometer – the raw luminescence image measured at 630 nm; c) the phosphor thermal image showing the measurement lines / areas. Bottom left: temperature error with thermal imaging (principally due to unknown emissivity) when sighted on the phosphor coating and emissivity set to 1, as a function of temperature. Bottom right: temperature error with thermal imaging when sighted on the bare metal; here the emissivity is much lower (i.e. the bare metal is shinier) which gives very large measurement errors. This shows how the phosphor can be used to both enhance the emissivity and also 'calibrate' the measurement i.e. deduce the emissivity *in situ* to correct the thermal imaging measurements.

*On-line thermometry for forging*

STRATH has developed emissivity-stable thermographic phosphor coatings for a dual phosphor / pyrometer thermometry system capable of providing reference temperature measurements to the dynamic correction of surface emissivity. Emissivity measurements carried out at AFRC have demonstrated the high stability of these phosphor coatings in the temperature range from 50 °C to 550 °C, bound to the stainless steel substrate. Currently the three-gate phosphor thermometer measurement system constructed at STRATH is limited to 550 °C due to the decreasing lifetime of the phosphor MFG:Mn. To increase the temperature range, experiments are ongoing to increase the ratio of phosphor to binder, while retaining the emissivity characteristics.

Other issues with the AFRC phosphor thermometer system have been overcome, including excessive bleed-through excitation (addressed by adding an additional optical filter) and coating degradation causing a slow reduction in the luminosity of the phosphor over several hours (a result of substrate-binder interaction, solved by using a different substrate).

The experimental layout for calibration of the phosphor is shown in Figure 4.1.5. Prior to calibrating the phosphor, coated stainless steel tokens were thermally cycled in a calibrated furnace. Following the thermal cycling, images were taken to calculate the decay time. The decay time at set temperatures was then fitted to provide a calibration curve of decay time as a function of temperature. The image temperature profile was calculated from the fit.

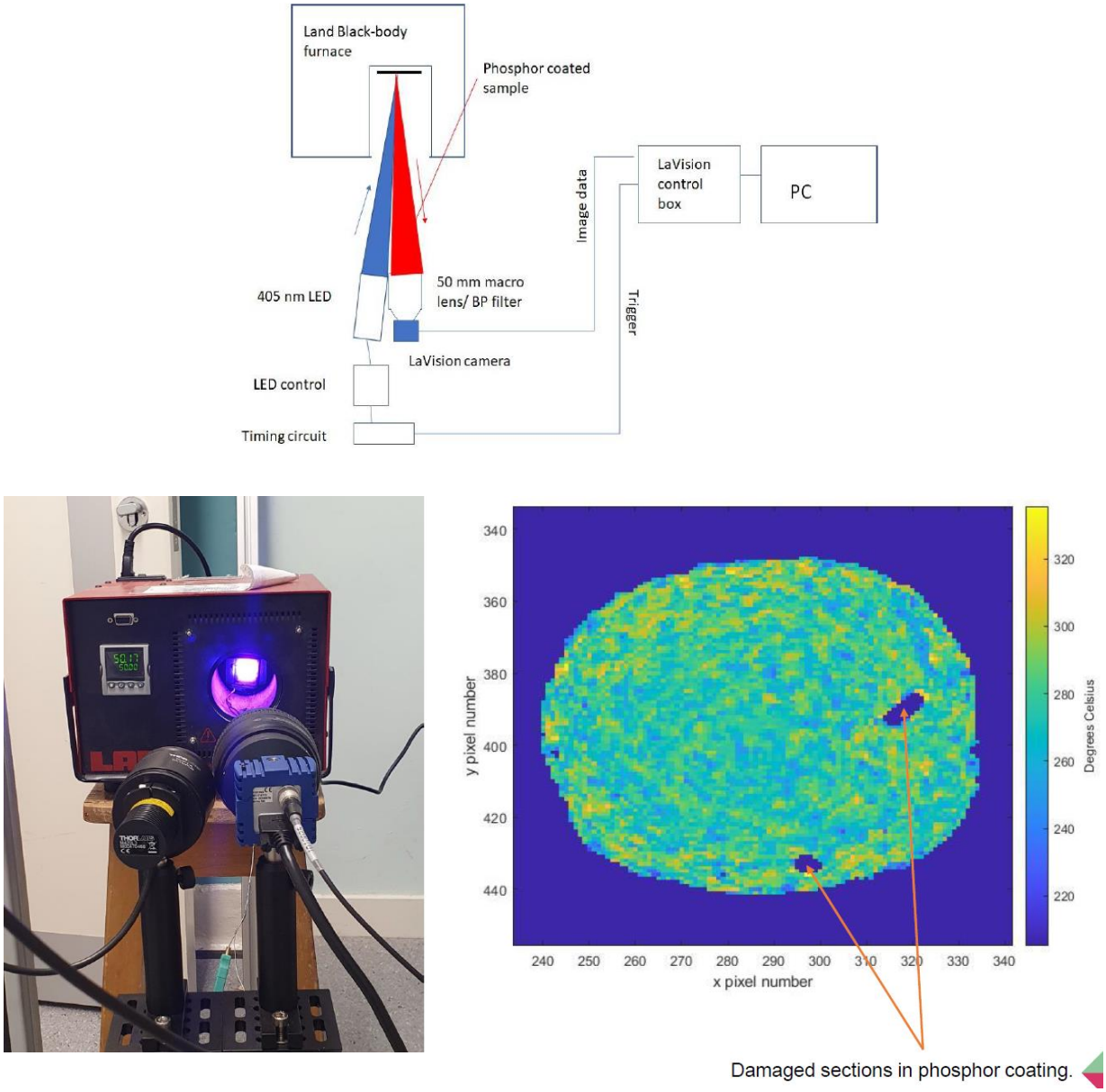


Figure 4.1.5. Top: Experimental layout for phosphor calibration. Bottom left: Experimental apparatus for on-line phosphor thermometry, in the process of being calibrated. Bottom right: Sample output from the on-line thermometry system.

The system is now able to perform continuous 'online' measurements during processes such as forming and forging at the AFRC. Methods for both on-line and off-line temperature measurements have been developed. On-line thermometry is used to monitor the temperature of the forging die during material processing.

Some trials were conducted on the 500 tonne hydraulic press manufactured by Precision Forging Technologies Ltd (Figure 4.1.6, top left). This is fitted with temperature controlled and heated plates designed to square material. The 500 tonne press is versatile and can be used for open and closed die forming operations, sheet forming and also cold forming of gears. The machine is fully controllable and is able to provide constant displacement speed, load or strain rate. Both top and bottom plates can be heated up to 400 °C with heating cartridges through separate PID control systems. This provides a large flat temperature-controlled surface to place three plate samples on, namely C42-MOD steel, aluminium and titanium TI35A, coated with phosphor (Figure 4.1.6, bottom left). The results are shown in the form of 2D temperature maps in Figure 4.1.6 (right).

The phosphor thermometry will be presented to AFRC members and deployed with the AFRC range of forming and forging processes to complement other temperature measurement techniques.

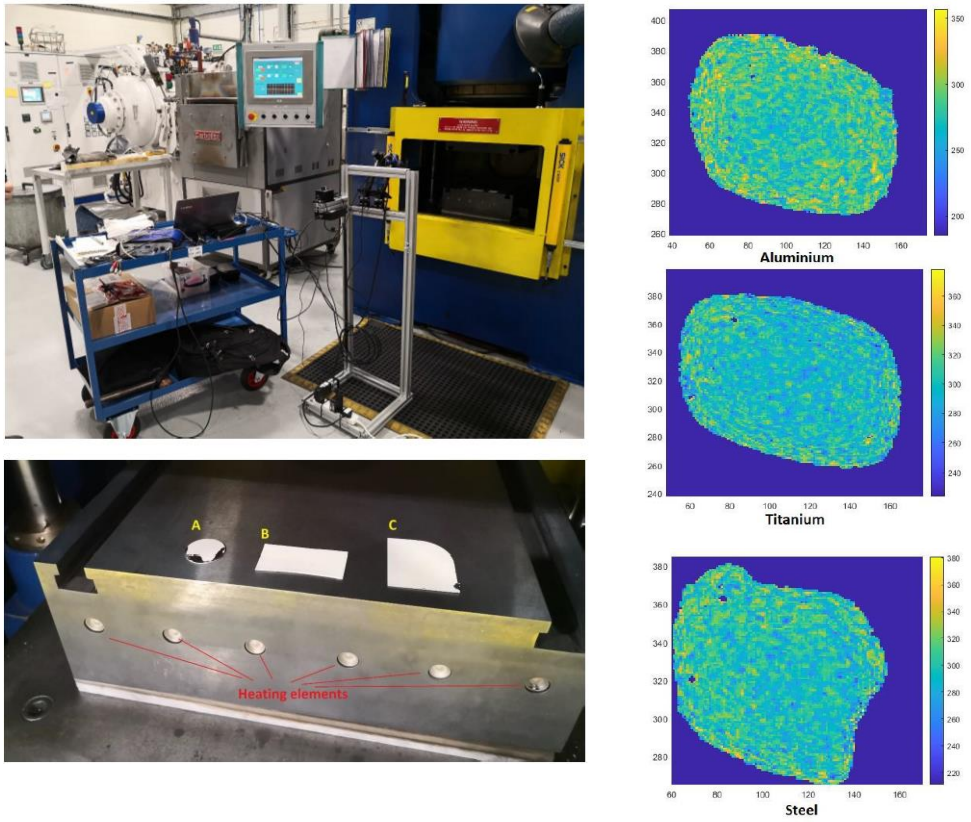


Figure 4.1.6. Top left: 500 tonne hydraulic press at AFRC with heated bottom die. Bottom left: Samples placed on the heated bottom die of the hydralic pressure; A) C42-MOD steel, B) aluminium and C) titanium TI35A. Right: three 2D images corresponding to the three samples, generated with phosphor thermometry at 300 °C.

*Off-line thermometry for forging*

Different phosphors are required for thermal history measurements. Commercial phosphors are good for on-line measurements, and coatings will now give repeatable results, but off-line thermal history measurements require the phosphor to undergo a permanent change. Currently, no commercial phosphors are available to purchase, but some companies do offer coatings that can be used. Yttrium orthosilicate was identified as a suitable high temperature host, with a melting point above 2000 °C. A terbium dopant was chosen for this as it give a strong green photoluminescent response with a long decay lifetime of greater than 2 ms for dopant concentration of about 10 %. The terbium doped yttrium orthosilicate (YSO:Tb in amorphous form) was made in-house using the sol-gel method. For thermal history applications, the phosphor must be crystallised in an oxygen-free atmosphere because the rare-earth dopant in phosphor reacts with atmospheric oxygen; the number of dopant ions participating in the reaction increases with temperature, causing a corresponding reduction in photoluminescent decay time. The experimental setup for the off-line phosphor thermometer is shown in Figure 4.1.7. Here, the phosphor was excited by a frequency quadrupled solid-state Nd:YAG pulsed laser. The signal is detected using a Thorlabs PDA-10A silicon photodiode fitted with a FL532-10 bandpass filter. The off-line phosphor thermometer was applied to forging dies and metal heat treatment applications to determine the maximum temperature experienced by the forging die.

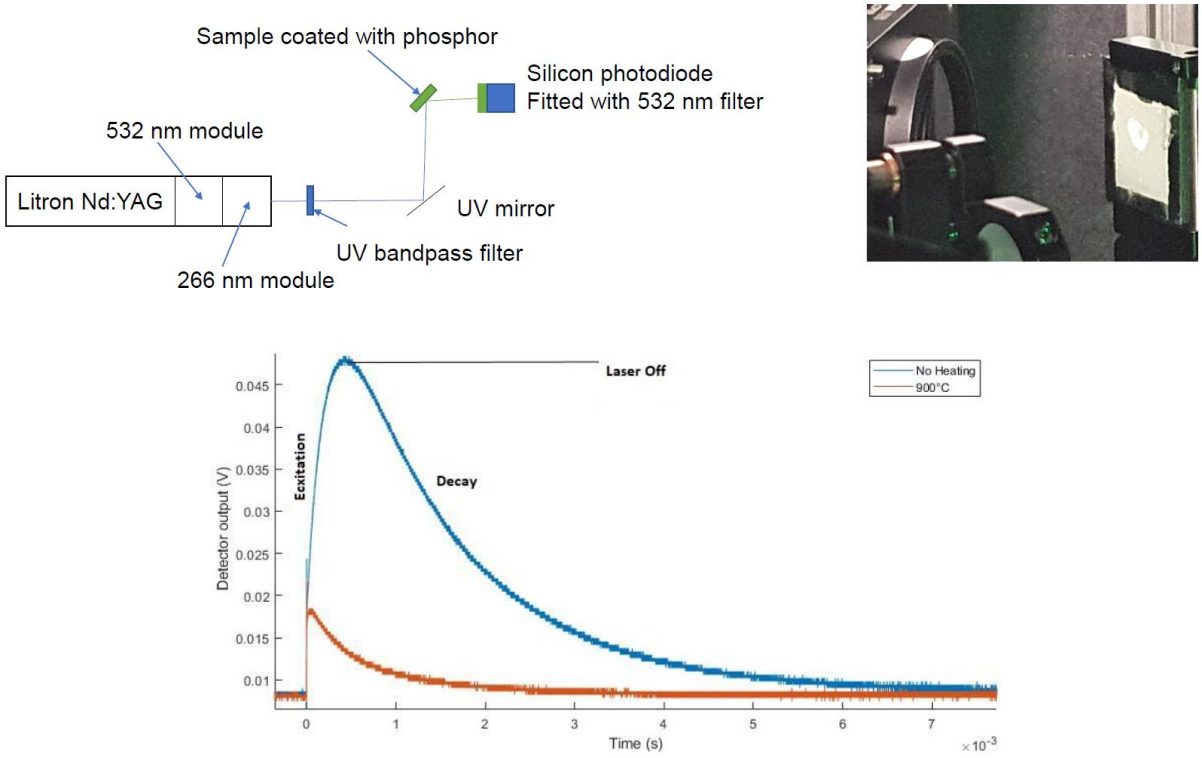


Figure 4.1.7. Top left: Experimental layout for the off-line phosphor thermometer. Top right: interrogation of a phosphor coating. Bottom: Luminous intensity as a function of time for the off-line thermometry system at room temperature (blue line) and at 900 °C (orange line).

Fibre-optic based measurement system for temperatures of up to 1000 °C in a braking system

The aim of this task is to study the influence of temperature, as measured at the interface of an automotive brake pad and disk by phosphor thermometry, on braking system properties. Good performance of a braking system is strictly dependent on the formation of a so-called friction layer or third body, which forms when a disk and pad come into contact during braking. The heat generation during braking affects the topology of the friction layer. This in turn induces phenomena such as material deformation that changes the contact pressure, whose uneven distribution is the main reason for uneven wear. The measurement of the temperature at the interface is therefore an aspect of paramount importance when forecasting the whole performance of a braking system.

INRIM developed an appropriate binding mechanism for good adhesion of a thick layer of the phosphor on at least one of the types of brake pad that is used in industrial applications (supplied by ITT). CNR advised on binder property constraints. The phosphor thermometer developed by INRIM was applied to the measurement of surface temperature in the brake testing rig at ITT's industrial facilities.

At INRIM the technique for preparing the phosphor coating has been refined by improving the phosphor/binder ratio, the thickness, and the curing process. A series of laboratory measurements were then performed to validate the phosphor temperature measurements on brake pads using the INRIM reference hot plate. A selected brake pad was machined: three bores with different depths were drilled and a Cr:YAP phosphor coating was applied to the bottom of each bore. The aim was to obtain, using phosphor thermometry, the temperature profile across the brake pad and consequently the temperature at the interface. Two calibrated Type N thermocouples were inserted at different depths in the body of the brake pad as well (see Figure 4.1.8).

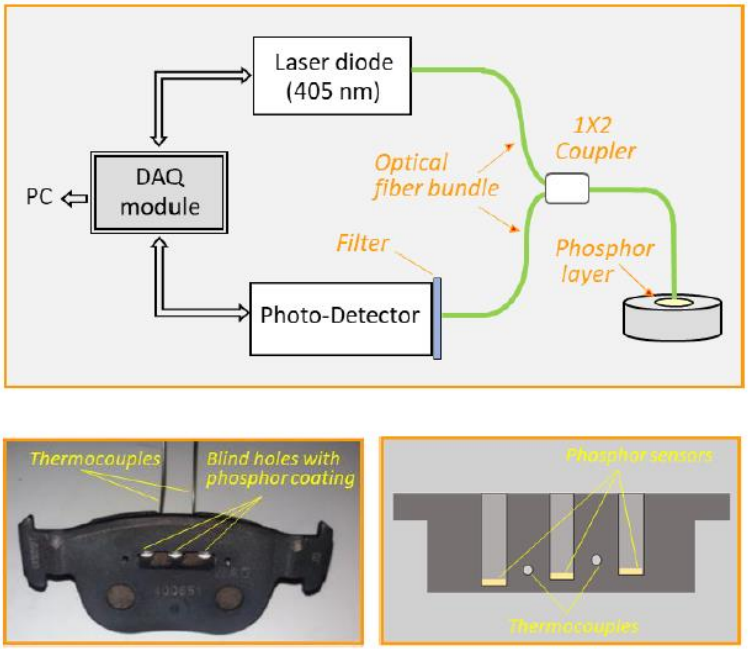


Figure 4.1.8. Top: INRIM phosphor thermometry setup. Bottom: Instrumentation of brake pad.

The brake pad was positioned on the reference surface of the hot plate and pressed against it by applying a combination of weights through a mechanical mechanism to ensure a reproducible contact force. A phosphor spot was also directly applied to the metal surface of the hot plate to provide a phosphor thermometry reference temperature. At several temperatures in the range from ambient to 200 °C, the reference temperature generated by the hot plate apparatus was compared to the phosphor reference temperature and to the extrapolated phosphor temperature (i.e. the temperature obtained by linear extrapolation of the three temperature readings across the brake pad). A linear relationship between the phosphor reference temperature and the hot plate reference temperature was observed, consistent with a thermal contact resistance which depends on the applied load on the brake pad.

The braking tests reached a disk temperature of about 600 °C. The results of the measurements showed that phosphor thermometry appears to give a more representative temperature at the interface between the brake pad and disk than is available with thermocouples due to very high heat dissipation rates, and suggests that thermocouples underestimate the temperature by several tens of degrees (see Figure 4.1.9). The phosphor thermometry technique therefore offers lower temperature measurement uncertainty of better than 3 °C. The instrumented brake pad has been exploited as a transfer standard for on-site measurements of surface temperatures in the brake testing rig at ITT's industrial facilities.

The surface of the pads and/or disks tested was analysed by CNR, in order to evaluate the friction layer formed, if any, and any changes in terms of composition, leading to potential material degradation. As the thickness of tribologically induced films is usually of the order of 1 μm or thinner, surface techniques are preferred. The analysis was carried out on brake pad at ITT. Scanning Electron Microscopy using the Energy Dispersion Spectroscopy probe (SEM-EDS) was used by CNR to determine the morphological and elemental composition, on both the surface and cross section of the worn materials (Figure 4.1.9). A new brake pad was analysed and the main constituents were observed (polymer as matrix, iron oxide, barite, aluminium oxide, carbon, steel, various sulphides and oxides, and others). Brake pads having the same composition as the new one, but having been subjected to two braking cycles at the facilities of ITT, were then analysed to assess the friction layer formed and changes in composition. The main changes consisted of surface oxidation and flattening/compression of some constituents at the surface. This information will be used to inform further development of the phosphor application methodology.

The project successfully achieved the objective with all these results.

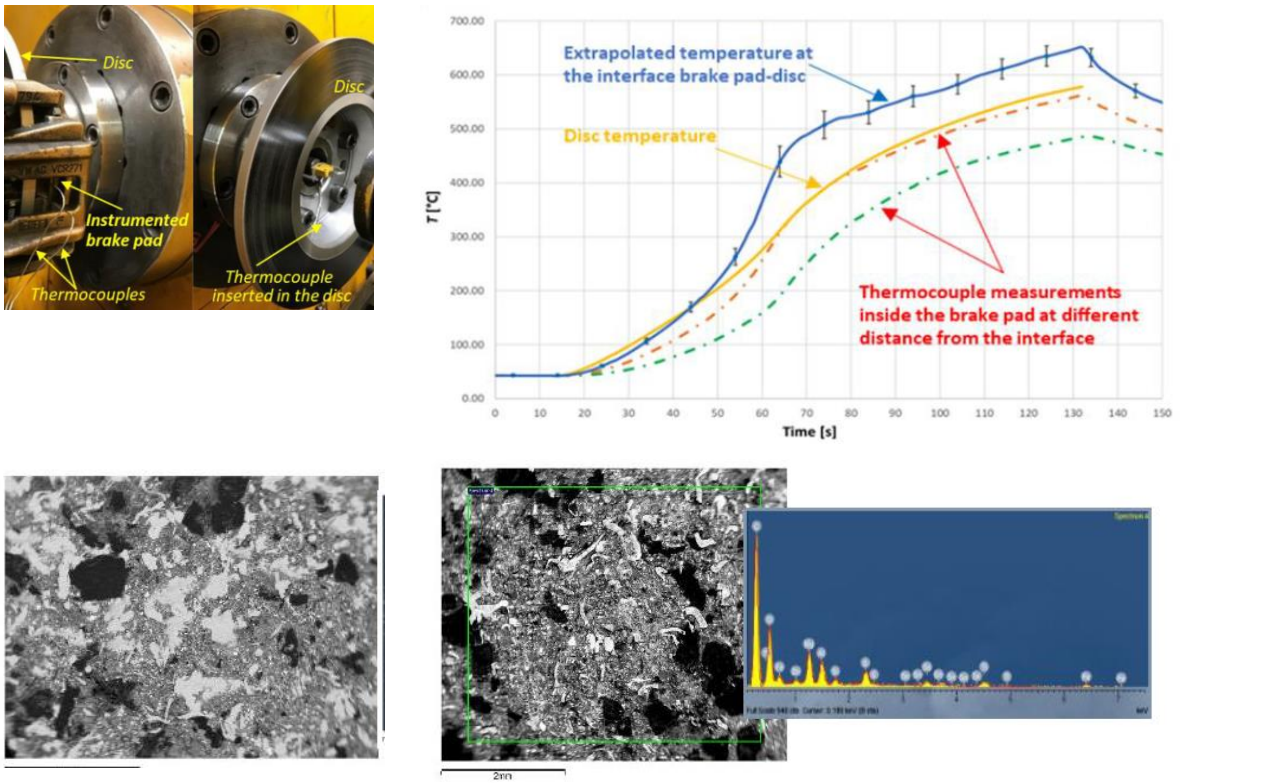


Figure 4.1.9. Top left: ITT test setup. Top right: braking test over a duration of two minutes; the rotational speed of brake disk was 70 rad/s and braking pressure was 12 bar. Bottom left: Chemical analysis of the worn pad showing the flattening of elongated particles emerging at the surface. $Fe_xO_y$ and carbon appear as predominant constituents of the tribofilm. Bottom right: Analysis of the new pad evidencing the complexity of composition and morphology.

### 4.2 Objective 2: Reduce uncertainty of temperature measurement in-process

***- through developing and implementing improved and traceable low-drift temperature sensors for enhanced process efficiency and improved temperature control. This will address the traceability of optimised Pt-Rh thermocouples, and a reduction in the uncertainty of new in-process temperature sensors such as the double-walled mineral-insulated, metal sheathed (MI) thermocouples through mitigating insulation resistance breakdown and drift effects. The uncertainty will be less than 3 °C up to 1300 °C for the MI thermocouples.***

In EMPRESS, a systematic investigation of a number of different Pt-Rh thermocouples showed that the most stable thermocouple consistent with readily available Pt-Rh wire compositions, at least in the temperature range 1324 °C to 1492 °C, is the Pt-40%Rh versus Pt-6%Rh thermocouple[6]. This is due to the combined effects of thermoelectric drift due to vaporisation of Pt and Rh oxides. A preliminary reference function was also drafted. In EMPRESS 2, to facilitate uptake of the new thermocouple type, NMIs have systematically determined its reference function. This builds on the development of high temperature fixed points[7] in FP5 project G6RD-CT-2001-00610 HIMERT[8], EMRP JRP IND01 HiTeMS[9] and EMPIR JRP 14IND04 EMPRESS. The utility of the optimised thermocouple will be demonstrated by trials in industrial furnace manufacturing, and other trials at collaborators' sites e.g. float glass manufacturing applications.

[6] Pearce J V, Edler F, Elliott C J, Garcia Izquierdo C, Kim Y-G, Martin M J, Tucker D, Veltcheva R I 2018, A systematic investigation of the thermoelectric stability of Pt-Rh thermocouples between 1300 °C and 1500 °C, Metrologia 55 558
[7] Pearce J V 2017, Extra points for thermometry, Nature Physics 13 104
[8] Machin G, Beynon G, Edler F, Fourrez S, Hartmann J, Lowe D, Morice R, Sadli M, Villamanan M 2003, HIMERT: a pan-European project for the development of metal-carbon eutectics as temperature standards, AIP Conf. Proc. 684(1) 285, DOI: doi: http://dx.doi.org/10.1063/1.1627139
[9] Machin G, Vuelban E, Sadli M, Edler F, Strnad R, Anhalt K, Pearce J, Siefert M 2016, The research outcomes of the European Metrology Research Programme Project: HiTeMS – High Temperature Measurement Solutions for Industry, Measurement **78** 168

A second part of the thermocouple activities concerns the double-walled mineral insulated, metal sheathed (MI) thermocouple developed by UCAM[10]. This is currently the subject of a collaboration between UCAM and CCPI aimed at commercialising the new MI thermocouple type, which exhibits thermoelectric stability approaching that of noble metal thermocouples, at least up to about 1200 °C. Some validation of the drift performance of Type K and Type N thermocouples with this format was performed by UCAM, and in an industrial vacuum furnace at AFRC, in EMPRESS. Further validation was urgently needed and was undertaken by synchronised measurements at several participating NMIs. This includes a systematic comparison of drift rates of dual-wall and conventional thermocouples, and a systematic optimisation of the wall geometry, specifically a determination of the optimum ratio of the two wall thicknesses. The progressive breakdown of the insulation resistance above 600 °C as the ceramic insulation becomes conductive, which causes measurement errors, was also studied.

Standardisation of Pt-40%Rh vs. Pt-6%Rh thermocouples

The aim of this task was to establish an emf-temperature reference function for Pt-40%Rh vs. Pt-6%Rh thermocouples in the temperature range between 0 °C and 1769 °C in air. This was based on a set of at least 5 (of 11 investigated) exceptionally thermoelectrically stable and homogeneous similar thermocouples or on one or two 'master' thermocouples. All required measurements were traceable to the ITS-90, based on measurements of the thermocouple electromotive force (emf) at fixed points and in comparison. The thermocouples were constructed by the partners. Additionally, the post-assembly heat treatment was optimised to reach the most stable thermoelectric conditions of the thermocouples.

Eleven Pt-40%Rh vs. Pt-6%Rh thermocouples were constructed by PTB, NPL, CEM, CMI and TUBITAK by using thermoelements which were provided by JM, and additional thermocouples were provided to UL and DTI. These were used in the reference function determination. In particular, an agreed post-assembly heat treatment was performed by PTB, CEM, CMI, NPL and TUBITAK to achieve optimum thermoelectric performance. PTB and NPL jointly prepared a measurement protocol to unify the pan-European measurement effort. A by-product of this activity was a revised EURAMET best practice guide on thermocouple calibration, incorporating new, documented information on typical thermoelectric homogeneity values for a range of thermocouples[11].

Using the facilities of PTB, NPL, CEM, CMI, DTI, TUBITAK and UL traceable measurements to the ITS-90 were performed at all ITS-90 fixed points, where available, and high temperature metal-carbon eutectic fixed points, and by applying comparison methods in the temperature range between 0 °C and 1769 °C in order to yield a large number of emf-temperature pairs. During these measurements, tests of the thermoelectric stability and homogeneity were performed repeatedly according to the agreed measurement protocol.

Ten of the eleven thermocouples met the specified stability requirements, which was a drift rate at the Cu point (1084.62 °C) less than 0.5 μV within 50 hours annealing at 1350 °C. The following general principles were applied for the reference function determination:

- Comparison measurements provide the most data points, and were therefore considered to be the key task for the determination of the reference function
- Fixed point measurements were performed to check the stability of the Pt-40%Rh/Pt-6%Rh thermocouples during the measurements by comparison, but were also used to determine the reference function
- Repeated homogeneity tests of the Pt-40%Rh vs. Pt-6%Rh thermocouples were performed

For each of the ten thermocouples, different numbers of temperature/emf pairs were obtained. The data of the thermocouples CEM-2018-1 and CEM-2018-2 covered the widest temperature range and the difference between them was smaller than the expanded uncertainty. Furthermore, they showed good thermoelectric homogeneity and stability. One condition to perform a least-squares fit to determine the emf-temperature relationship of a thermocouple is that all data are from one thermocouple or the data are from a set of statistically indistinguishable thermocouples. Therefore, based on all data measured, the data of the CEM thermocouples were chosen for the construction of the reference function.

The resulting reference function was subject to considerable analysis, which arrived at a final solution of two polynomials, one from 0 °C to 660.323 °C (the freezing point of aluminium), and another one above

[10] Scervini M and Rae C 2013, An Improved Nickel Based MIMS Thermocouple for High Temperature Gas Turbine Applications, Journal of Engineering for Gas Turbines and Power, 135 091601, DOI: 10.1115/1.4024420

[11] Pearce J V, Arifovic N, Bojkovski J, Edler F, de Groot M, Garcia Izquierdo C, Kalemci M, Strnad R 2020, Calibration of thermocouples: EURAMET Calibration Guide No. 8 Version 3.0 (online only https://www.euramet.org/publications-media-centre/calibration-guidelines/)

660.323 °C. The reference function relates the thermoelectric voltage emf in units of μV to the temperature *t* in units of °C:

$$emf = \sum_{i=0}^{n} a_i \cdot t^i$$

The polynomial coefficients are shown in Table 4.2.1. The uncertainty associated with the reference function was also carefully analysed, and is shown in Figure 4.2.1. Detailed information on the measurement conditions (temperature ranges of the comparison measurements, apparatus, standard thermometers and fixed points used, as well as full results, are presented in[12].

| coefficients | below Al | above Al |
|---|---|---|
| $a_0$ | 0 | 71435.3813 |
| $a_1$ | 0.137315647 | -568.1009491 |
| $a_2$ | 0.006333794 | 1.941456131 |
| $a_3$ | -3.65645E-06 | -0.003686384 |
| $a_4$ | 8.80882E-09 | 4.29132E-06 |
| $a_5$ | -1.13502E-11 | -3.12896E-09 |
| $a_6$ | 5.40932E-15 | 1.39612E-12 |
| $a_7$ | | -3.48828E-16 |
| $a_8$ | | 3.73963E-20 |

Table 4.2.1: Reference function coefficients.

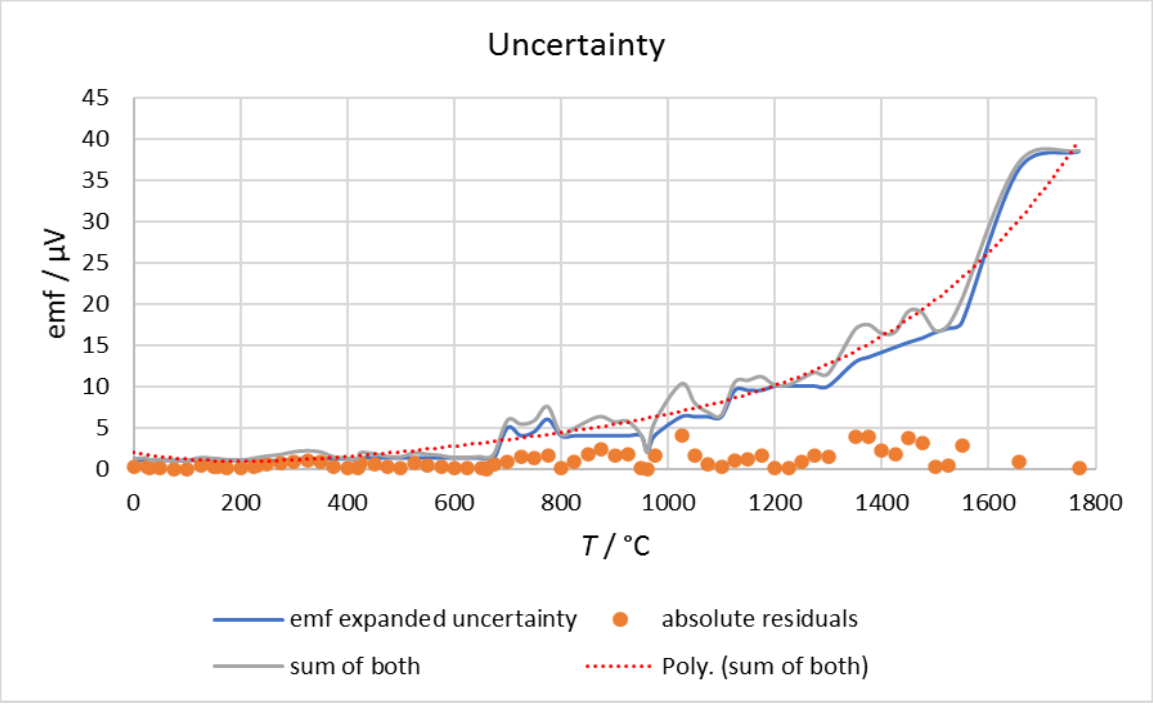


Figure 4.2.1: Uncertainty of the reference function.

[12] Edler F, Bojkovski J, Garcia Izquierdo C, Martin M J, Tucker D, Arifovic N, Andersen S L, Strnad R, Zuzek V 2021, Pt-40%Rh versus Pt-6%Rh thermocouples: an emf-temperature reference function for the temperature range 0 °C to 1769 °C, Int. J. Thermophys 42 150

A number of trials of the Pt-40%Rh vs. Pt-6%Rh thermocouples in industrial conditions were performed. This includes float glass manufacturing up to 1550 °C in Denmark, quartz glass manufacturing in the UK, industrial furnace and ceramic fibre manufacturing at MUT, and trials in a steel manufacturing facility in the Czech Republic, to demonstrate the achieved stability of the thermocouples and validity of the new emf-temperature reference function. These are described below in the section 'Industrial trials and early uptake of thermocouple thermometry'.

Optimisation of the stability of dual-walled MI thermocouples up to 1200 °C

The aim of this task is to optimise the design of double-walled MI thermocouples and to establish the basis for the standardisation of the double-walled MI thermocouples of types K and N. Comparison tests were executed using double-walled MI thermocouples to find an optimal inner to outer wall thickness ratio. In addition, a suite of double-walled MI thermocouples were constructed and investigated in comparison with conventional MI thermocouples of the same type. The results will provide the basis for approaching standardisation bodies (see the Section below 'Dissemination to standards bodies and other committees') which will open up the opportunity to use the sensors widely in industrial applications.

All measurements for the comparative metrological characterisation of dual-wall and conventional MI thermocouples of the same geometry (3 mm outer diameter) of Type K and N with regard to their thermoelectric stability and homogeneity have been completed. For this investigation, two different measurement protocols were realised among the six partners. Three partners performed isothermal drift tests of the MI thermocouples at 1200 °C and three partners performed thermal cycling drift tests of the MI thermocouples between 300 °C and 1150 °C, each against thermoelectrically stable reference Type R and Type S thermocouples. In addition, calibrations of the Type K and N thermocouples were performed at the Fe-C eutectic fixed point before and after the two different thermal treatments to verify drift effects. Furthermore, the thermoelectric homogeneity of the Type K and N thermocouples was verified at 200 °C in liquid baths. For the electromagnetic field tests, eight MI thermocouples were tested: four Type N thermocouples (two conventional and two dual-wall) and four Type K thermocouples (two conventional and two dual-wall). The thermocouples were tested at 5 different temperatures: -196 °C, 0 °C, 125 °C, 250 °C and 500 °C.

To investigate the influence of different geometries of Type K and N dual-wall thermocouples on their performance compared to equivalent conventional and 'standard' dual-wall thermocouples, the following three different alternative designs were investigated: one 'thin wall' design, with wall thickness smaller than 'standard' geometry, and two 'thick wall' designs, with two wall thicknesses larger than 'standard' geometry. Two different test methodologies, similar to the measurement protocols described above, were used to assess the drift of the thermocouples. In addition, metallurgical investigations of Type N thermoelement samples in an electron microscope were carried out using WDS (Wavelength Dispersive X-Ray Spectroscopy) to measure the local elemental composition inside the two thermoelements. In this way, a possible qualitative correlation of the drift results with respect to geometry (sheath thickness) and impurities in the thermocouple wires could be identified.

The following findings can be summarised for Type N thermocouples. The dual-wall thermocouples can outperform the conventional thermocouples when a suitable geometry is selected. In particular, the standard dual-wall and thick sheath dual-wall designs show better drift performance in the isothermal tests than conventional Type N thermocouples. Only the 'thin wall' dual-wall thermocouples have shown a larger drift compared to conventional thermocouples. Testing in thermal cyclic conditions exacerbates the drift of conventional thermocouples, and using electron microscopy techniques, a higher level of contamination has been detected in conventional thermocouples when tested in thermal cyclic conditions compared to isothermal tests. The drift of the dual-wall thermocouples seems to be largely insensitive to thermal cycling conditions. On the other hand, the dual-wall thermocouples have shown a tendency to fail when subject to severe and prolonged thermal cycling conditions. This is not unexpected considering that the outer layer made of Inconel 600, which has the function of protecting the sensing elements from the environment, is thinner compared to the sheath thickness of a conventional thermocouple.

Although different geometries of dual-wall thermocouples were designed and manufactured to identify the effect of geometry on the drift of the sensors, it was not possible to identify a clear relationship between drift and the inner wall thickness ratio. The drift results of the different sensors (in particular the standard dual-wall and both of the 'thick wall' dual-wall designs) differ only to a limited extent.

For the Type K thermocouples, two different batches were tested. The results can be summarised as follows. Different compositions of Type K thermoelements induce different performance in terms of drift. This applies to both conventional and dual-wall thermocouples. The different batches of dual-wall thermocouples tested have performed marginally better or worse than conventional Type K thermocouples with thermoelements of

the same composition. These results are in contrast with previous results obtained from other batches of dual-wall Type K thermocouples previously tested independently at UCAM and CCPI. The reason for this discrepancy is not clear and would require further investigation. It can be stated that, across the thermocouple Types K and N investigated, the best performing dual-wall design in terms of drift and durability is the second 'thick sheath' dual-wall for Type K thermocouples, while the standard dual-wall design was the best approach for the Type N thermocouples. This may suggest that the best dual-wall geometry may differ for different thermocouple types. The uncertainty was seen to be less than 3 °C for both dual-wall and conventional single-wall MI thermocouples. Selected examples of the thermoelectric drift tests are shown in Figure 4.2.2.

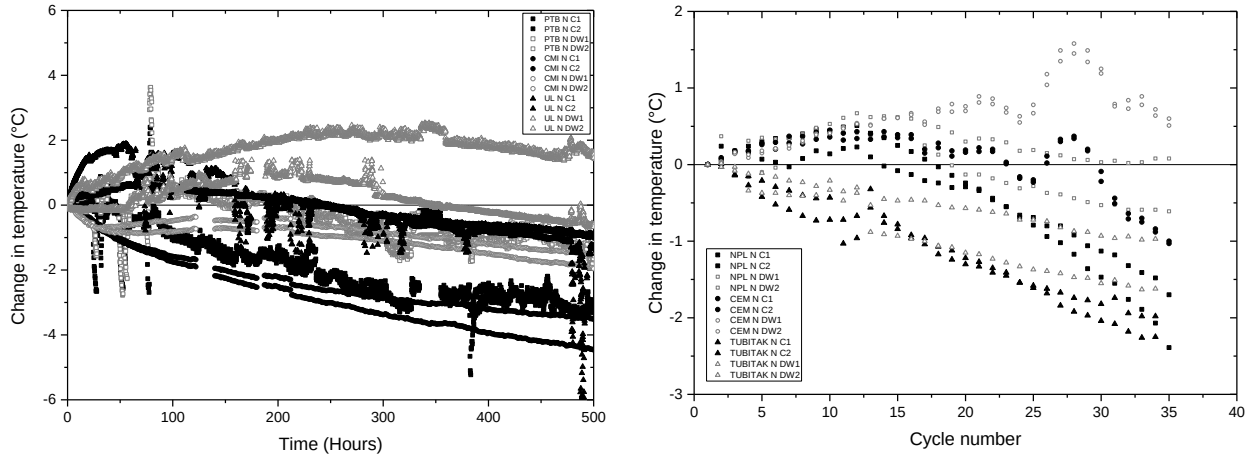


Figure 4.2.2: Representative plots of the thermoelectric drift of MI Type N thermocouples as a function of elapsed time during isothermal high temperature exposure (left panel) and during thermal cycling tests between 300 °C and the selected high temperature (right panel).

Assessment of the insulation resistance breakdown of MI thermocouples up to 1300 °C

The aim of this task is to investigate the issue of insulation breakdown for MI thermocouples and to perform measurements of the insulation leakage of double-walled and conventional MI thermocouples of types K and N. There is evidence that, under particular conditions, conventional thermocouples experience insulation resistance breakdown at high temperatures. When using dual-walled thermocouples, it can be assumed that due to the lower insulation layer thickness because of the limited space in dual-walled thermocouples, the resistance breakdown can even occur at lower temperatures or shorter operating times compared to conventional thermocouples. Measurement schemes were devised to improve the characterisation of this effect by UCAM, CCPI, NPL and CEM.

The insulation resistance of a cohort of representative MI thermocouples was characterised at temperatures up to 1160 °C, with simultaneous measurements of the error in indicated temperature by *in situ* comparison with a reference Type R thermocouple. Intriguingly, there appears to be a systematic relationship between the insulation resistance and the error in the indicated temperature. At a given temperature, as the insulation resistance decreases, there is a corresponding increasingly negative error in the temperature measurement. Although the measurements have a relatively large uncertainty, the trend is apparent at all temperatures above 600 °C becoming progressively more pronounced as the temperature increases, which suggests that it is real. Furthermore, the correlation disappears at temperatures below about 600 °C, which is consistent with the well-established diminution of insulation resistance breakdown effects below that temperature. In fact, the extrapolated error for zero insulation resistance was found to increase with temperature, providing solid evidence that the measurement error is indeed indicative of insulation resistance and can in principle be used as an indicator. This raises the intriguing possibility of using the as-new MI thermocouple calibration as an indicator of insulation resistance breakdown: large deviations of the emf in the negative direction could indicate a correspondingly low insulation resistance.

As it was not clear if additional insulation resistance breakdown (due to e.g. contamination or other microstructural change) could occur early in the life of the sensor or at very long exposure time, it was decided by UCAM and CCPI to expose the sensors for prolonged times at different temperatures while monitoring the insulation resistance continuously, which was measured between one wire and the sheath of the thermocouple. This approach was used in order to maximise the probability of detecting possible insulation resistance breakdown, even in cases when this would happen temporarily. Furthermore, the temperature signal of the thermocouples under test was measured concurrently to detect abrupt or progressive changes in

insulation resistance, which could suggest insulation breakdown. Several tests were undertaken using conventional Type K thermocouples to induce insulation breakdown, including isothermal tests ranging from 800 °C to 1300 °C and severe thermal cyclic tests with maximum temperatures of 1100 °C, 1200 °C and 1300 °C. Insulation breakdown was detected in one case during an isothermal test at 1300 °C, but the condition could not be reproduced in multiple repetitions of the same test. It can be concluded that additional insulation resistance breakdown (above and beyond that caused by the well-known decreased resistance as a function of temperature) is likely a very rare event considering that it was impossible to obtain sensors after operation in the field that had experienced this, and considering the very numerous thermocouples tested during EMPRESS 2 with almost no failures during extensive testing.

Dissemination to standards bodies and other committees

**IEC:** The International Electrotechnical Commission is an international standards organization that prepares and publishes international standards for all electrical, electronic and related technologies, collectively known as "electrotechnology". A key task is to provide evidence to the IEC committee TC 65/SC 65B/WG5 responsible for the MI thermocouple standard IEC 61515[13] that the stability of double-walled MI thermocouples is superior to that of conventional single-walled thermocouples. A further difficulty with compliance of the double-walled MI cables with the IEC 61515 standard is the reduced cross-sectional area within the thermocouple due to the thicker wall. This means there is less space for the thermoelements which impedes compliance with the geometrical specifications. Evidence of superior stability, even with reduced thermoelement size and spacing, is needed before modifications to the geometrical requirements of IEC 61515 can be proposed. A report on the performance of the Type K and N dual-walled mineral insulated, metal sheathed thermocouples was sent to the chair of IEC/TC/SC 65B/WG5 to facilitate discussion at the next committee meeting.

In addition, a report on the pan-European determination of the reference function of Pt-40%Rh vs. Pt-6%Rh thermocouples, identified as having optimum thermoelectric stability above about 1200 °C, was submitted to the chair of IEC/TC/SC 65B/WG5, to prepare the ground for introduction of a new thermocouple type in IEC 60584-1.

**ASTM:** ASTM International is an international standards organisation that develops and publishes voluntary consensus technical standards for a wide range of materials, products, systems and services. The ASTM E585 Standard for Specification for Compacted Mineral-Insulated, Metal-Sheathed, Base Metal Thermocouple Cable specifies strict dimensional, geometrical and form factor tolerances on this type of thermocouple cable, which is difficult for the new dual-walled thermocouples examined in EMPRESS 2 WP2 to comply with. One member of UCAM made representations to the E20.12 – Thermocouples Specifications committee in November 2018 to suggest modifications to the standard to include the dual wall thermocouples in the ASTM E585 standard. Further independent validation provided by EMPRESS 2 will support the proposal.

**CCT:** The Consultative Committee for Thermometry is concerned with the establishment and realisation of the International Temperature Scale of 1990 (ITS-90) and thermodynamic temperature, and ensuring temperature measurement equivalence worldwide. Via the Task Group 'Guides on Thermometry' (TG-GoTh), a number of guides are in the pipeline which incorporate outputs from EMPRESS 2. Guides under development include:

- CCT Guide on Secondary Thermometry: Industrial Platinum Resistance Thermometers (led by NPL) – submitted to CCT secretary and circulated to CCT members for comments
- CCT Guide on Secondary Thermometry: Thermocouples I: General Usage (led by PTB) – published[14]
- CCT Guide on Secondary Thermometry: Thermocouples II: Calibration and reference thermocouples (PTB, NPL) – currently under development

**SAE/NADCAP:** SAE International is a global association of more than 128,000 engineers and related technical experts in the aerospace, automotive and commercial-vehicle industries, and has a strong influence over regulatory standards in those sectors. Nadcap was set up by SAE International and is a worldwide cooperative program of major companies designed to manage a cost-effective consensus approach to special processes and products and provide continual improvement within the aerospace and defense industries.

Close liaison with this standards body is essential in order to gain traction for the new dual-walled thermocouples in the aerospace sector, due to its heavy regulatory requirements for any new instrumentation product.

One member of the CCPI team attended the SAE AMS AMEC Aerospace Metals and Engineering Committee meeting in Port Huron, Michigan, USA. 17/18th July 2019. Meetings covered heat treatment and potential

[13] IEC 61515:2016 Mineral insulated metal-sheathed thermocouple cables and thermocouples
[14] https://www.bipm.org/en/committees/cc/cct/guides-to-thermometry

revision of the AMS 2750 specification in the light of the deviation from the standardised cross-sectional geometry of the double-walled mineral insulated, metal sheathed thermocouples of WP2. The thermoelectric stability measurements in WP2 will inform future meetings with this standards body. Additionally, one member of UCAM presented the project activities to the Heat Treating Task Group (HTTG).

Industrial trials and early uptake of thermocouple thermometry

*Quartz glass manufacturing*

Heraeus Conamic manufacture quartz components for subsequent manufacture of a wide range of products including raw quartz (tubes, plates, ingots, etc.), quartz glass components for fabrication of microchips, composites for computers and mobile devices, optical components for fibre-optics, lenses and microlithography, specialty fibre components for medical, industrial and sensing applications, and tubes for laser applications.

The basic process is to take quartz in powder form and melt it in order to produce an extruded solid quartz glass product. The furnace typically used for this is shown in Figure 4.2.3. The process temperature can be between 1800 °C and 2000 °C. Temperature measurement and control is an essential part of the process, because the viscosity of glass changes rapidly with temperature; if the glass is too viscous or not viscous enough the extrusion is readily deformed and must be discarded. This means there is a narrow temperature window of about 20 °C. Measurement of the temperature is extremely difficult and is done with a combination of pyrometers and thermocouples, but even thermocouples can be unreliable at these temperatures because their stability is affected by the high temperatures. Pyrometry is also unreliable because the emissivity of the furnace materials is poorly characterised, and measurements exhibit large variations from one operator to another. The optimum solution so far is to mount thermocouples in the die at the base of the melting pool, which is at a temperature of about 1650 °C. To improve the thermocouple stability, the EMPRESS 2 Pt-40%Rh vs. Pt-6%Rh thermocouple was mounted in the die alongside existing Type B thermocouples. The thermocouple was kept *in situ* during a processing run, and its output, together with an adjacent Type B thermocouple, is shown in Figure 4.2.4. This shows that the thermocouple is sufficiently robust in this harsh environment, and maintains the required stability. Unfortunately, for operational reasons the process was stopped before reaching the higher processing temperatures up to 1700 °C, so the performance at those temperatures could not be assessed in time. Nonetheless, it has been demonstrated that the new high stability thermocouple is sufficiently robust for implementation in this process setting.

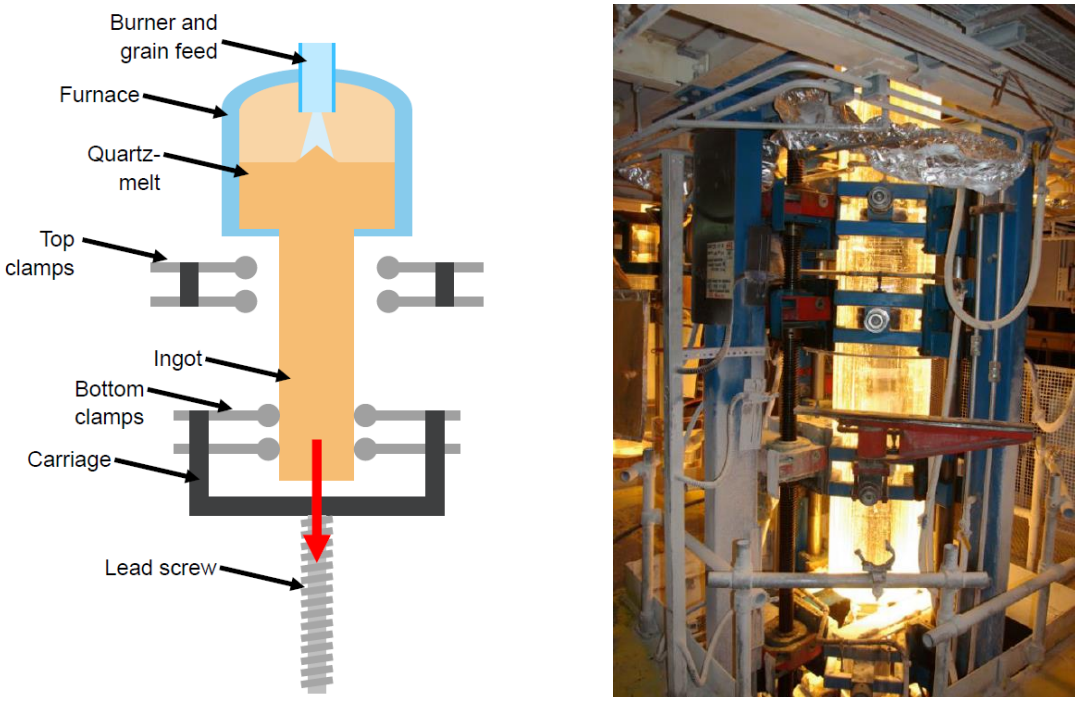


Figure 4.2.3. Quartz glass furnace. The thermocouples are mounted in the die towards the top of the furnace.

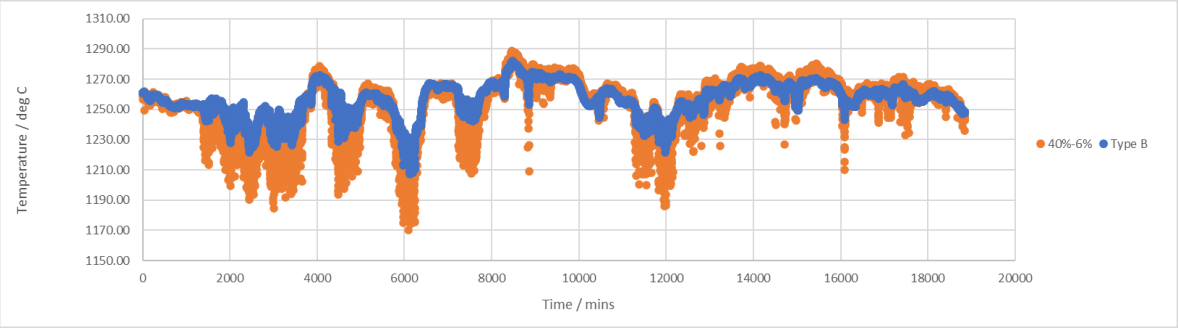


Figure 4.2.4. Output of Pt-40%Rh/Pt-6%Rh thermocouple (orange points) and an adjacent conventional Type B thermocouple. The wider temperature excursions of the Pt-40%Rh/Pt-6%Rh thermocouple are real and due to the slightly different location.

*Steel production*

Bonatrans is a company in Bohumín in the Czech Republic dealing with the railway industry, with a focus on designing and manufacturing high quality wheelsets for trains. The Pt-40%Rh vs. Pt-6%Rh thermocouple was installed in a high temperature furnace used for heat treatment of steel ingots prior to further processing. The thermocouple was installed in a four-bore ceramic tube together with a standard Type S thermocouple (normally used). The assembly was in turn inserted into a protective ceramic tube.

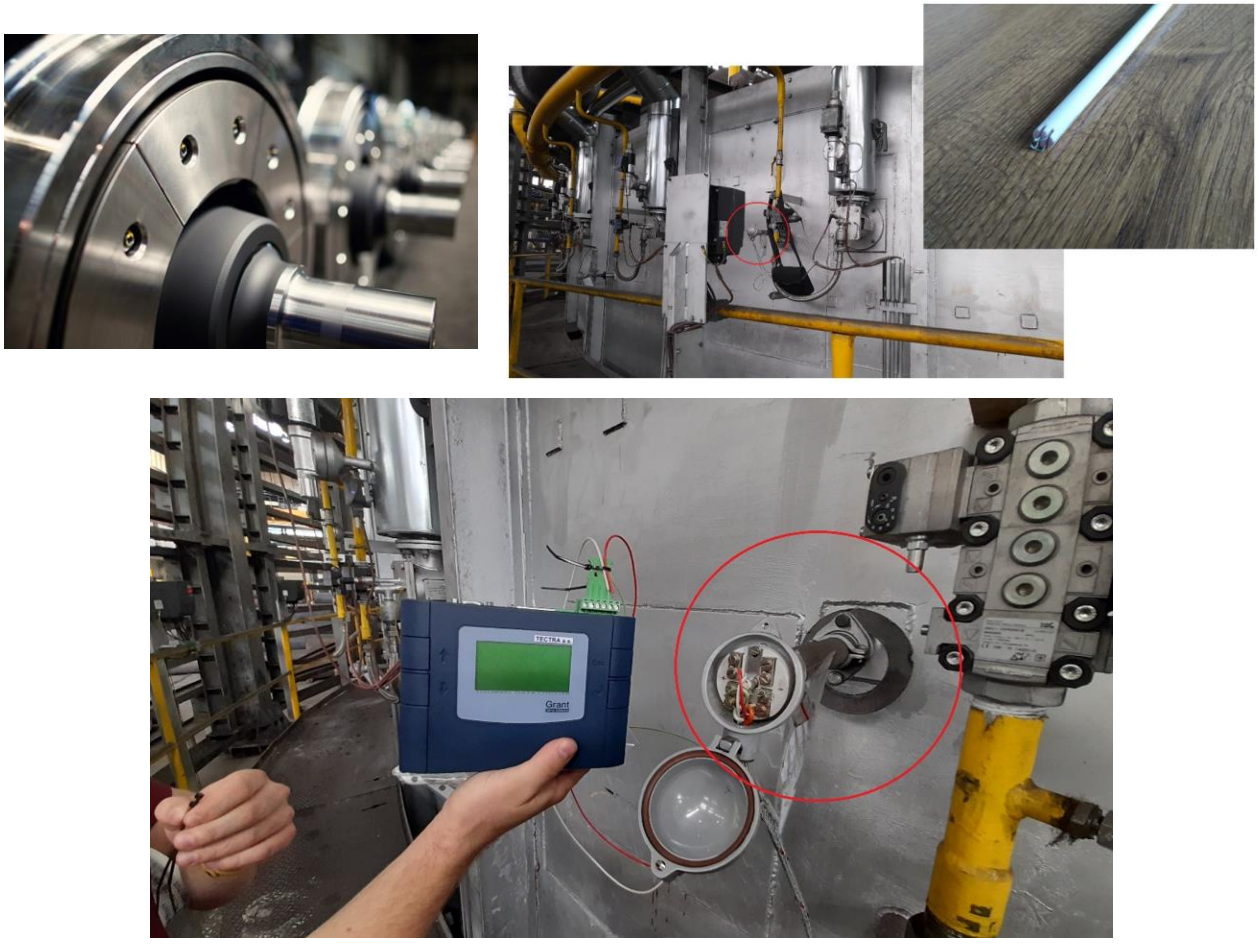

Figure 4.2.5. Top left: steel train wheel component produced by Bonatrans. Top right: external wall of the heat treatment furnace with thermocouple assembly emerging from the furnace; inset: thermocouple assembly with protective tubes removed. Bottom: detail of thermocouple assembly on external wall of furnace (encircled in red), with associated instrumentation.

The operating temperature of the furnace was 1270 °C, and the test took a total of 16 days. Both thermocouples were connected to an industrial Grant Squirrel datalogger type SQ2010. The reference function published as part of EMPRESS 2[15] was used to convert the thermocouple emf to temperature for the novel thermocouple. Figure 4.2.5 shows some images of the heat treatment furnace setup and instrumentation.

Both thermocouples were in agreement within 1 °C over the duration of the test. Although the novel thermocouple is designed for use at higher temperatures where the standard thermocouples are subject to more severe thermoelectric drift, the test was very useful for proving the concept, to show that the novel thermocouple is fit for purpose in terms of installation, compatibility with existing instrumentation, and robustness. Some results are shown in Figure 4.2.6.

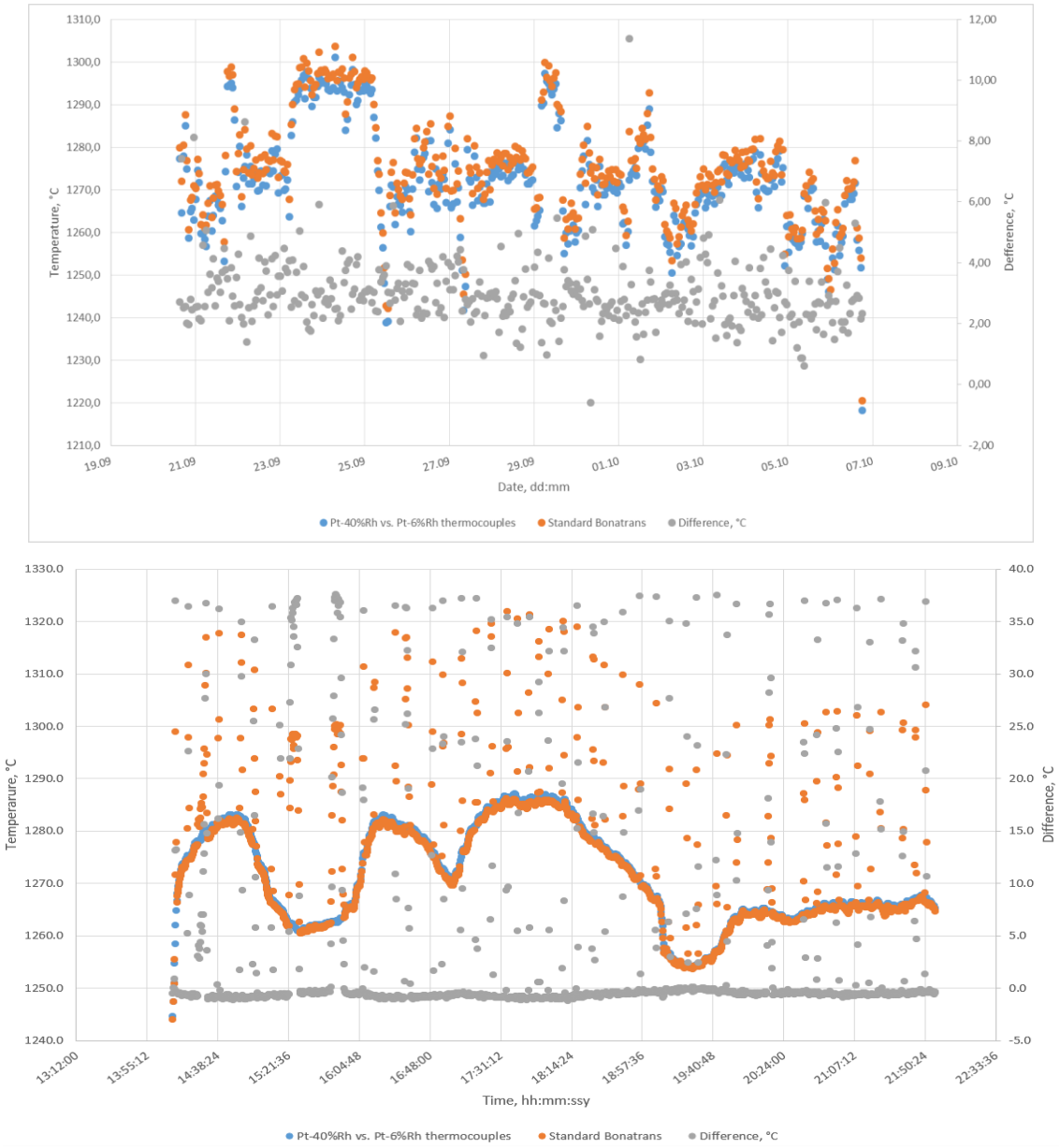


Figure 4.2.6. Two examples of the temperature indicated by the standard (orange) and novel (blue) thermocouples as a function of time during different furnace programmes.

[15] Edler F, Bojkovski J, Izquerdo C G, Martin M J, Tucker D, Arifovic N, Andersen S L, Sindelarova L, Zuzek V, Pt-40%Rh versus Pt-6%Rh thermocouples: an emf-temperature reference function for the temperature range 0 °C to 1769 °C, Int. J. Thermophys. 42 150 (2021)

*Float glass manufacturing*

Field trials were conducted by DTI at Ardagh Glass Holmegaard A/S (AGH) to assess the robustness of the Pt-40%Rh vs. Pt-6%Rh thermocouples under harsh environmental conditions in floating glass at temperatures up to approximately 1300 °C.

To ensure appropriate protection of the Pt-40%Rh vs. Pt-6%Rh thermocouples over time when inserted into the floating glass environment at AGH, it is important to protect the sensor from degradation by installing it into additional protection sheaths compared to the standard ceramic protection tube in which the sensor is installed during calibration. The two thermocouple wires were welded at the tip of the sensor and installed in a double-bore, open-end ceramic protection tube. The sensor was then calibrated traceably at DTI to provide traceability to the ITS-90. This calibration was performed in an additional single-bore, closed-end ceramic protection tube. For installation into the floating glass another single-bore, closed-end protection tube was used during the trials at AGH as seen in Figure 4.2.7 (left). For an enhanced lifetime of the ceramic sheath a platinum coating could have been applied; however, this was not done for the current installation, where the sensor was expected to be installed in the floating glass at AGH for only 2-3 weeks.

To reduce the thermal stress of the sensor as it is installed in the approximately 1300 °C floating glass, the sensor is preheated on top of the furnace as shown in Figure 4.2.7. This is the normal procedure for installation of high temperature thermocouples at AGH. To provide access to the floating glass of the furnace, an insulating brick of the furnace can be removed as seen in Figure 4.2.7. The sensor can then be inserted into the floating glass and the thermoelectric voltage can be measured. Usually, AGH uses multiple measurement points when measuring and controlling the temperature of the furnace, and the sensor was installed in the vicinity (within 1 metre) from a permanent process control sensor (Type R thermocouple) which is used as a reference. The installation of the thermocouples, and the cold junction in the initial setup, are shown in Figure 4.2.8.

Figure 4.2.7: Left: the thermocouples are installed in ceramic protection tubes. Centre: the thermocouples are preheated on top of the furnace prior to installation to minimize the thermal stress upon installation. Right: access to the floating glass is provided by removing one of the bricks of the furnace.

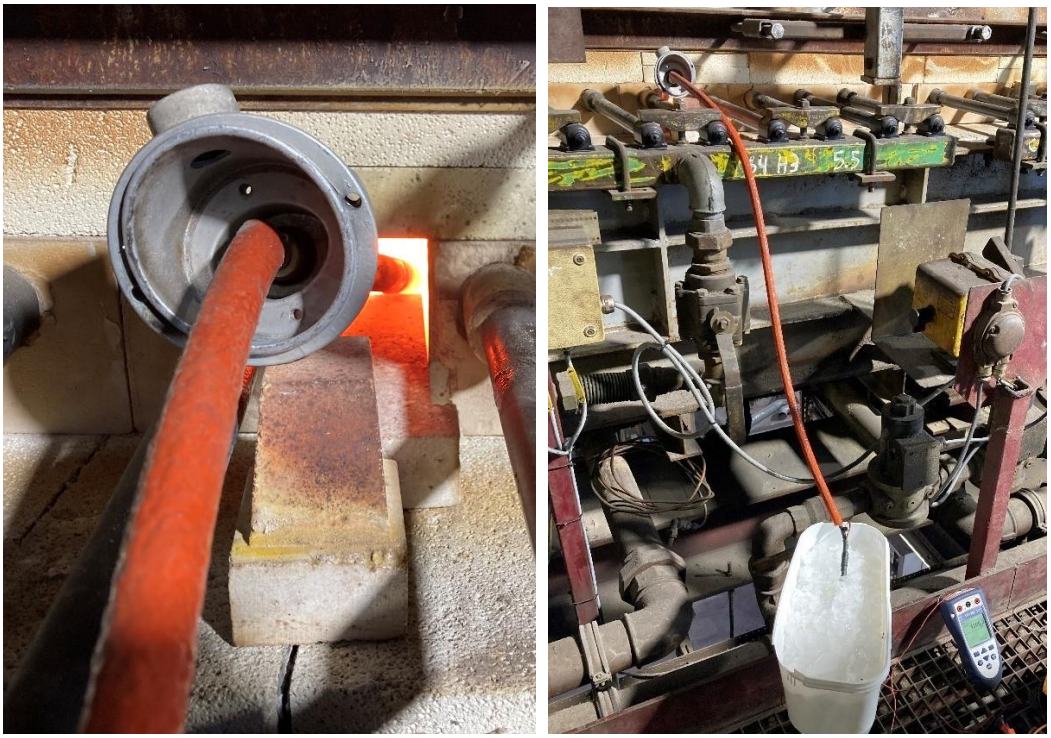

Figure 4.2.8: (left) sensor as installed in the floating glass at approximately 1300 °C, (right) the sensor installation in the glass is seen at the top of the picture and here the cold junction can also be seen.

It was not practical to extend the Pt-40%Rh vs. Pt-6%Rh thermocouples to the furnace measurement and control system to obtain long-term logging directly traceable to the ITS-90. However, AGH made a set of Type R thermocouple wires available for this purpose. This resulted in uncontrolled fluctuations in the measured thermoelectric voltage due to the varying cold junction temperature, which amounted to a few degrees. As the principle aim of this test was to verify the robustness of the new thermocouple, this was deemed acceptable.

The long-term temperature logging was then conducted. The new thermocouple and the nearby Type R control thermocouple can be seen to be in good agreement (Figure 4.2.9), with the temperature difference between them almost certainly due to the temperature gradient across the region of the furnace separating them.

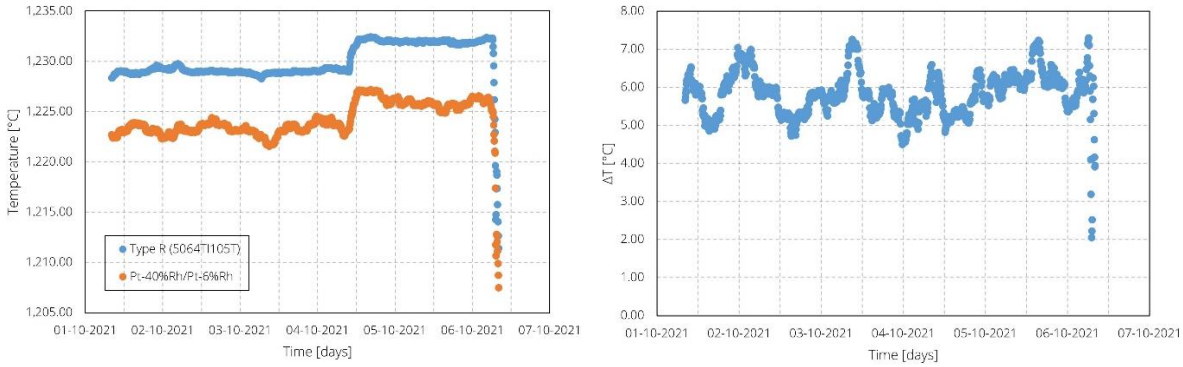


Figure 4.2.9: Measurements every six minutes for the Pt-40%Rh vs. Pt-6%Rh thermocouples from 1st October to the 6th October and compared with a permanently installed Type R thermocouple (ID: 5064TI105T). Left: absolute values. Right: the difference between the two sensors (see text).

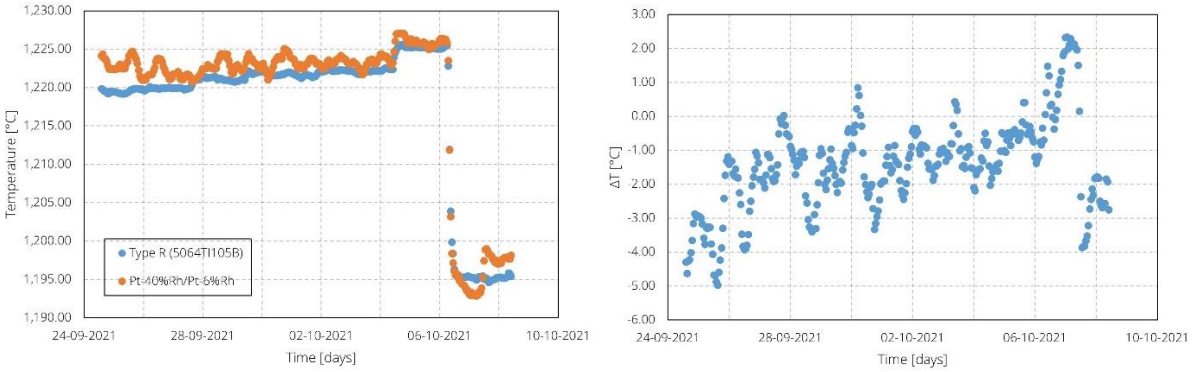


Figure 4.2.10: Measurements every hour for the Pt-40%Rh vs. Pt-6%Rh thermocouples from 24th September to the 8th October and compared with a permanently installed Type R thermocouple (ID: 5064TI105B). Left: absolute values. Right: the difference between the two sensors (see text).

To assess this, the output of the new thermocouple was compared to that of a closer control Type R thermocouple, as shown in Figure 4.2.10. The agreement was found to be even closer. The fluctuations in measured temperature seen in Figure 4.2.9 and Figure 4.2.10 are probably due to variation in the temperature for the first cold junction. However, the overall trend of the new thermocouple shows good stability over a period of 14 days, and the thermocouple was very responsive; the indicated temperature changes clearly correlated with changes in the temperature of the floating glass as measured by the established Type R control thermocouple.

*Industrial furnace manufacturing*

MUT Advanced Heating GmbH is a company based in Jena, Germany, which manufactures high temperature furnaces for industrial processing. It offers individual solutions in the field of heat treatment with expertise in development, engineering and production. Temperature measurement and control is a crucial part of high temperature furnace operation and has a strong influence on the quality of products processed within.

To test the utility of the Pt-40%Rh vs. Pt-6%Rh thermocouple an integrated hood furnace with internal dimensions (length by width by height) of 1.35 x 0.35 x 0.75 m was used for the experimental setup; this is shown in Figure 4.2.11. The thermocouple was placed near the heater and tested under a nitrogen atmosphere. The furnace has the following properties:

- Production furnace for integrated debinding and sintering of ceramics in a nitrogen atmosphere for debinding and in an air atmosphere with air purging up to a maximum temperature of 1650 °C
- Heating elements are Molybdenum disilicide
- Heating rate is between 5 °C per minute and 10 °C per minute
- The mass of the contents to be treated is up to 300 kg
- The volume of the chamber is about 1100 litres
- The atmosphere is air or nitrogen with a 1-5 mbar overpressure
- Gas flow is vertically upwards
- The material in the hot zone was alumina fibre ceramics
- The furnace is permanently cooled with water (the case is cooled)
- The furnace can be cooled down rapidly with a side channel blower (gas streaming to the interior)

The Pt-40%Rh vs. Pt-6%Rh thermocouple was mounted in an assembly and connected alongside the existing Type B thermocouple at that point as shown in Figure 4.2.11.

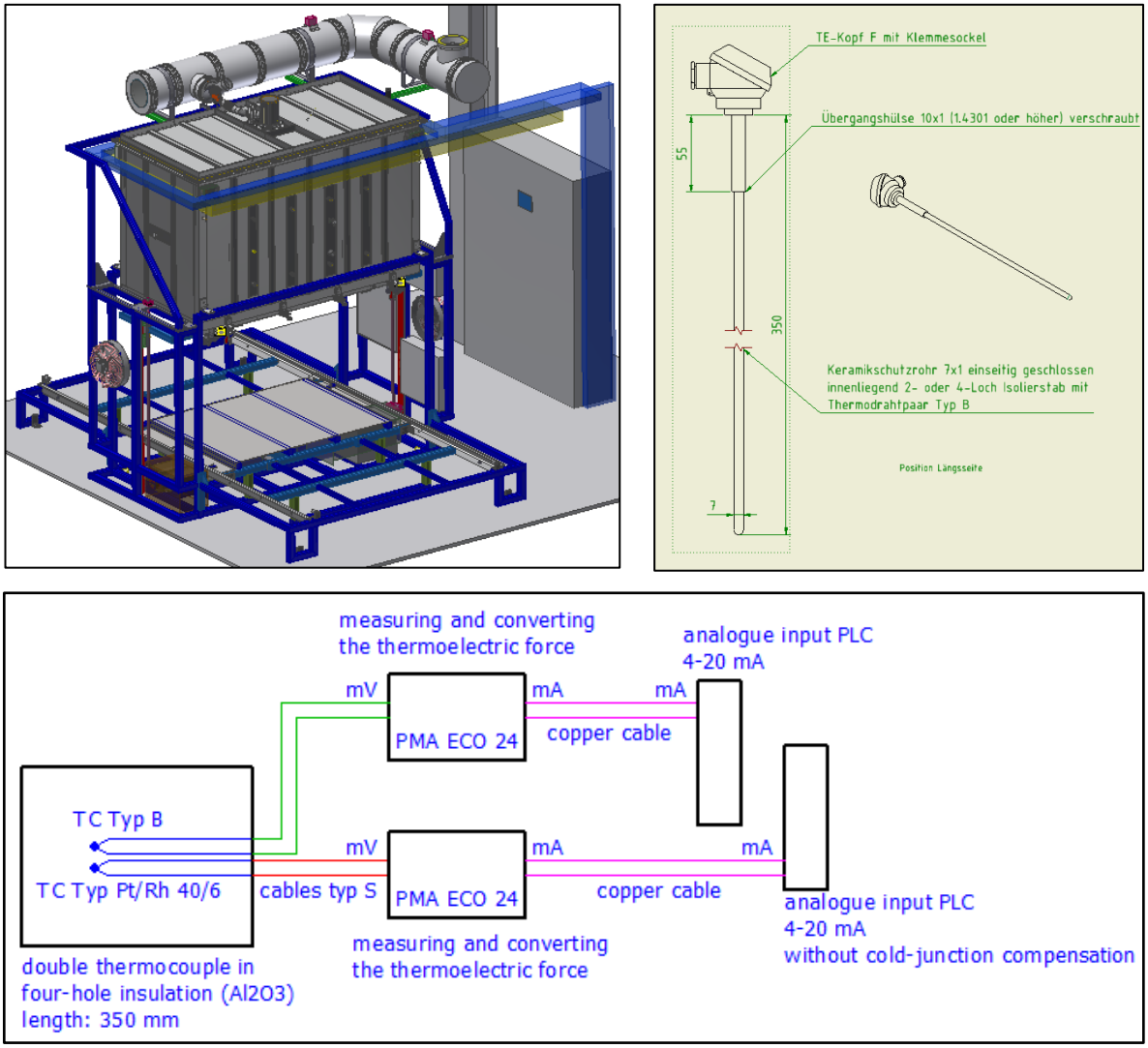


Figure 4.2.11: Top left: industrial hood furnace manufactured by MUT. Top right: thermocouple assembly. Bottom: thermocouple connection scheme.

The test programme examined the thermocouple output over several regimes:

- To 555 °C with 150 l/min $N_2$ (1-2 mbar overpressure)
- To 800 °C with 65 l/min $N_2$ and 10 l/min air (1-2 mbar overpressure)
- To 1600 °C with 20 l/min air (1-2 mbar overpressure)
- Cooldown with 30 l/min air (1-2 mbar overpressure)

Unfortunately because of staff limitations at MUT it was not possible to complete the test programme, but an example of a temperature cycle up to 1600 °C is shown in Figure 4.2.12. However, it was demonstrated that the thermocouple is sufficiently robust, and it is feasible to incorporate it in existing logging systems.

The project successfully achieved the objective with all these results.

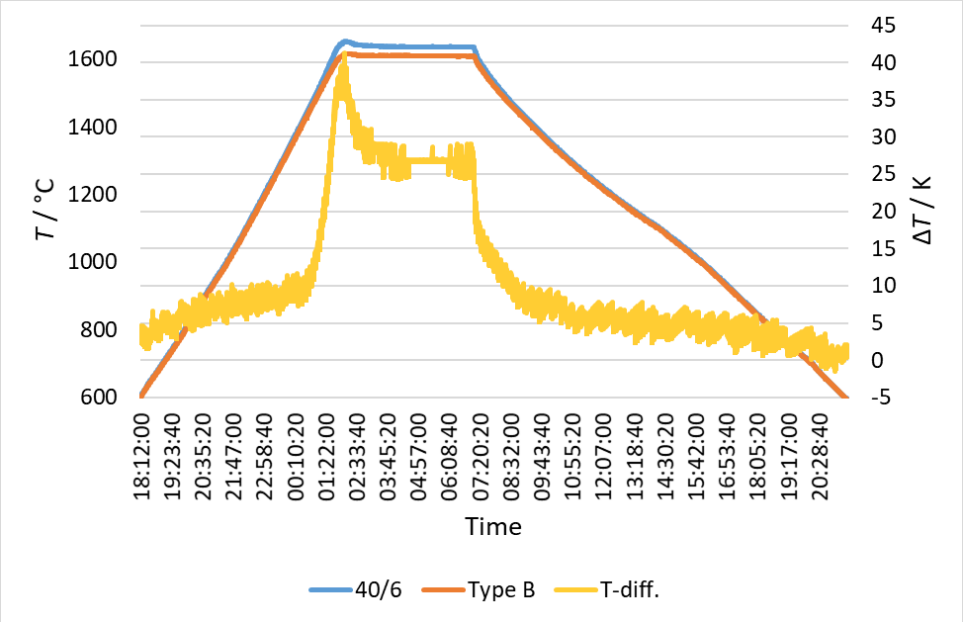


Figure 4.2.12: Comparison of Pt-40%Rh vs. Pt-6%Rh thermocouple output versus existing furnace-mounted Type B thermocouple during a temperature cycle from room temperature to 1600 °C, showing comparable output; the apparent temperature difference is probably due to the temperature gradient. This is significant given the displacement of the two sensors.

### 4.3 Objective 3: Implement *in situ* traceable combustion thermometry

***- by validating an in situ combustion reference standard (standard flame) of known temperature with an in-process target uncertainty of less than 0.5 %. In addition, to use the combustion reference standard to evaluate the linkage between portable standard reference flames, improved process temperature control, and an enhancement in process efficiency.***

In 14IND04 EMPRESS a portable standard flame was developed. By having a very well characterised gas composition and a judiciously designed geometry, the flame has a stable, spatially uniform temperature profile, and can be transported to end-users' sites to validate flame and combustion thermometry systems[16].

The flame system has been fully commissioned and is available as a measurement service to external customers. Using laser Rayleigh scattering, it has been possible to determine the post-flame temperature with an uncertainty of less than 0.5 % of temperature – this is a factor of two less than the original target uncertainty of 1 % of temperature. The flame and laser interrogation system are shown in Figure 4.3.1. Additionally, the system can provide a number of fixed and reproducible temperatures and species concentrations for propane/air equivalence ratios from $\phi$ = 0.8 (lean flame) to $\phi$ = 1.4 (rich flame). The range of (fixed) highly uniform temperatures that can be attained (dependent on $\phi$) is between 2050 K and 2250 K. This provides a robust mechanism to not only validate third party optical techniques but also assess their linearity. Measurements made by UC3M/CEM using a hyperspectral imager show excellent agreement with the standard portable flame (Figure 4.3.2), validating the technique and leading the way for development of a low-cost instrument in EMPRESS 2. Measurements made by DTU using IR/UV spectroscopy are equally impressive, showing outstanding agreement with the NPL measurements. Additionally, comparison of the measured and modelled IR emission spectra by DTU allowed further improvement of the temperature profile characterisation performed by NPL. This demonstrates the value of collaborating on this type of activity. Figure 4.3.2 also shows the reproducibility of the flame temperature as measured after each journey to the partners' laboratories.

[16] Sutton G, Fateev A, Rodriguez-Conejo M A, Melendez J, Guarzino G 2019, Validation of emission spectroscopy gas temperature measurements using a standard flame traceable to the International Temperature Scale of 1990, Int. J. Thermophys. 40 99

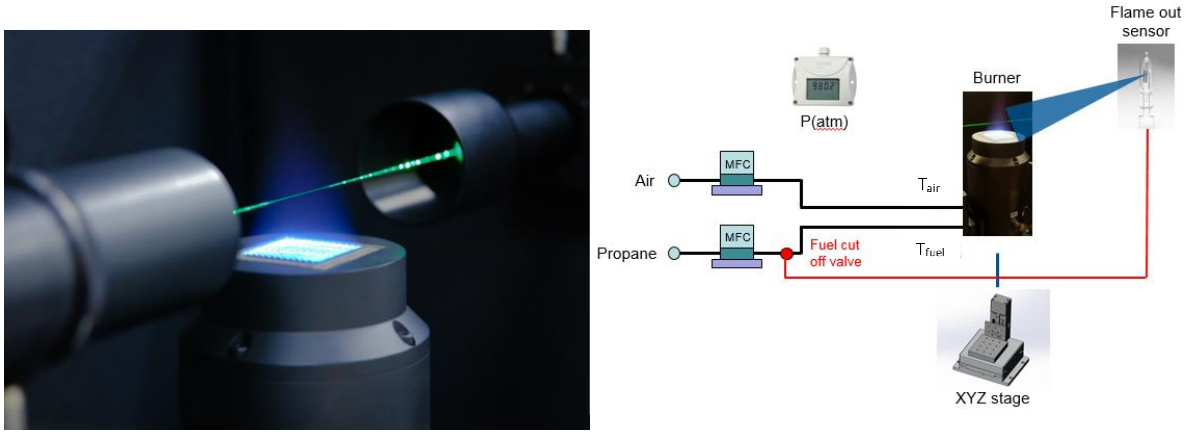


Figure 4.3.1. Left: Portable standard flame being interrogated by the NPL laser Rayleigh scattering apparatus. Right: The gas metering and burner control system.

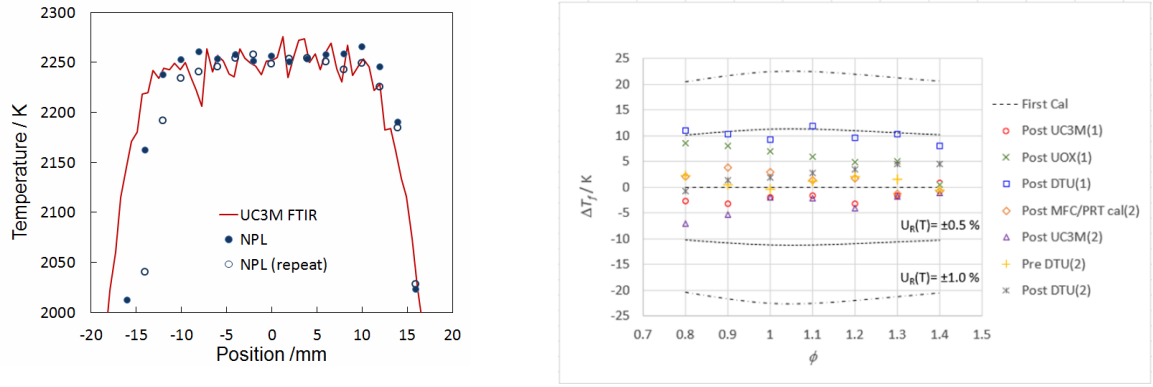


Figure 4.3.2. Left: Comparison of the spatial flame temperatures measured by NPL (Rayleigh scattering: open and closed circles) and UC3M/CEM (hyperspectral imaging, red line) at 20 mm above the burner surface. Right: Shift in flame temperature as a function of $\phi$ following measurement campaigns at UC3M, UOXF and DTU. Original calibration at NPL is zeroed (dashed line).

The idea of using the NPL portable standard flame is 1) to have a high temperature calibration source which can be used for absolute calibration of e.g. thermal imaging or sweeping systems based on gas thermal emission, and 2) to have a tool for optimisation and fine tuning of the above mentioned systems, so uncertainties in temperature retrievals with use of the standard flame are less than 5 %. In general, by providing an ideal, well characterised, uniform region of temperature, given by the standard flame, it is possible to calibrate other industrial combustion thermometers (e.g. pyrometers) under similar conditions.

In EMPRESS 2 the flame was used to facilitate the development of two new practical flame thermometers. The first, a low-cost (i.e. thousands of euros rather than tens of thousands) multi-spectral imaging system for flames, was developed and calibrated against the standard flame, then demonstrated in industrial applications e.g. fire resistance testing and natural gas production. The second device is an infrared on-sight/sweeping IR emission measurement system that can measure the 2D temperature profiles in flames or hot flue gases. This has been calibrated against the standard flame (which was re-validated at NPL before and after sending to each partner using laser Rayleigh scattering[17]), and demonstrated in a $NO_x$ selective non-catalytic reduction process.

[17] Sutton G, Levick A, Edwards G, Greenhalgh D 2006, A combustion temperature and species standard for the calibration of laser diagnostic techniques, Combustion and Flame 147(1-2) 39

*Development of a low-cost thermal imaging system*

The aim of this task is to develop a multispectral thermal imaging system that is suitable for temperature measurements in various industrial applications with overall uncertainties better than 0.5 %. The system uses a multi-filter based concept incorporated with an IR imaging camera.

Hot $CO_2$ and $H_2O$ are the major combustion products and give rise to strong thermal emission in the mid-infrared (1.5 μm to 5 μm) spectral range. The spectral distribution of the $CO_2$ and $H_2O$ emission depends on the molecules' temperature and the gas density. By measuring the emission spectra over selected $CO_2$ and $H_2O$ bands in the mid-infrared with a Fourier-transform Infrared (FTIR) spectrometer, and by comparing this with the known temperature-dependent emission spectra for each species determined *a priori*, the temperature and the density of gas in the optical path can be deduced. Using a FTIR spectrometer equipped with an InSb array detector, 2D maps of species and temperature can be produced. This 'hyperspectral' thermometry method has already been validated with the NPL portable standard flame, and it yielded temperature measurements in agreement with those obtained by Rayleigh scattering within about 0.5 % (see Figure 4.3.2).

These measurements require use of an expensive hyperspectral imager and are time-consuming, so UC3M, Sensia and DTU have pioneered a simplified technique that dispenses with the need to resolve individual spectral lines, relying instead on an iterative approach whereby low resolution spectra are measured over a set of relatively wide wavelength bands, which are selected using a set of six different filters. This is referred to as 'multispectral' thermometry. The measurement is then compared with simulated spectra generated using the HITEMP2010 database[18] which contains necessary spectroscopic information for spectra simulations. By iteration, the simulated spectrum is parameterised until it agrees with the measured spectrum, and in this way the temperature and $CO_2$ and/or $H_2O$ density can be deduced.

The practical consequence of this is that instead of measuring the spectral radiance of the gas with a large and costly high resolution spectrometer, an inexpensive low resolution device can be used with a set of filters to select different wavelength bands in turn. This low-cost method has been validated against the high resolution FTIR measurements, again by using the NPL portable standard flame as a reference. A map of the temperature profile of the flame obtained with the two methods is shown in Figure 4.3.3.

One remarkable outcome of this work is that temperature values retrieved with four or even two spectral bands are nearly as accurate as the values obtained with all six filters normally used, which confirms the feasibility of a cheaper IR camera-based system for stand-off industrial applications, achieving uncertainty of better than 0.5 % of temperature.

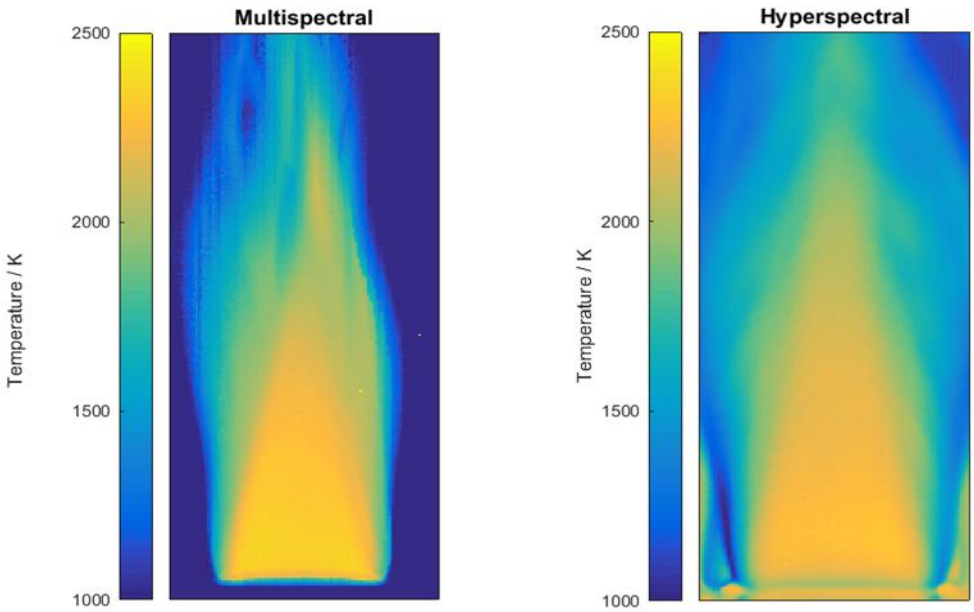


Figure 4.3.3: Temperature of the standard flame (average over the optical path being viewed) obtained using the low-cost multispectral imaging (left) and the (ten times more expensive) high resolution hyperspectral imaging (right), showing agreement within about 4.5 %.

[18] L. S. Rothman et al., "HITEMP, the high-temperature molecular spectroscopic database", J. Quant. Spectrosc. Radiat. Transfer 111, 2139-2150 (2010). See also https://hitran.org/hitemp/

*Development of a sweeping emission measurement system to improve waste incineration processes*

$NH_3$/urea solutions added to combustion gases at an optimum temperature can significantly reduce harmful $NO_x$ emissions using a selective non-catalytic reduction process (SNCR). However, this is most effective only in a narrow temperature range. One application of this is in waste incineration, and use of a high resolution FTIR, calibrated against the NPL portable standard flame, was demonstrated by DTU, in collaboration with Øresundskraft and Babock & Vølund, at the Filbornaverket waste incinerator plant in Sweden. The challenge was to improve the thermometry – in process – to facilitate better temperature control within a 20 °C temperature window in order to minimise $NO_x$ emissions from the incineration process.

An existing fast Infrared (IR) CEDIP camera with an InSb detector array has been serviced and upgraded for faster data acquisition. The camera was tested in combination with a small IR-grating spectrometer (upgraded with two new gratings optimised in the 1800 $cm^{-1}$ to 2900 $cm^{-1}$ and 2800 $cm^{-1}$ to 4500 $cm^{-1}$ spectral ranges) on the NPL portable standard flame and the results were compared with those obtained in the EMPRESS project with the high-end FTIR spectrometer. Excellent agreement in the overall spectra measurements was found. It was concluded that a more compact grating spectrometer with 1D image array would be a good alternative to the FTIR-based one, giving good spectral coverage, fast acquisition time and having no moving parts. With new commercially available 1D arrays it will open possibilities for future sensor developments. It has been shown that a machine learning approach to retrieve the gas temperature for normal and lean combustion cases (which are of most interest for practical applications) yields accuracies of 0.23 % and 0.21 % in temperature retrievals respectively[19] - considerably less than the target uncertainty of 0.5 %.

DTU and B&W Vølund, with support from the Filbornaverket WeT plant (Swedish waste incineration plant owned by the energy company Øresundskraft) have made preliminary measurements using a high-end FTIR spectrometer and a manually driven sweeping probe at the Filborna WeT plant. The measurements were made along a path close to the $NH_3$ injection[20] point (cross-section 10 m by 4.8 m, temperature about 1000 °C). An existing access port was used. The measurements have been made at various line of sight angles including -90°, -45°, 0°, 45° and 90° (0° is the horizontal cross-stack direction, 90° is parallel to the vertical wall). Measurements were made at high and low plant operation loads. Two spectral resolutions (2 $cm^{-1}$ and 8 $cm^{-1}$) with the fast scanning FTIR mode (100 kHz) were used for IR emission measurements in the spectral range 1000 $cm^{-1}$ to 6000 $cm^{-1}$. The system (FTIR spectrometer and probe) was calibrated using a calibrated portable blackbody at 875 °C. The sweeping measurements were supplied by on-site (permanently installed) thermocouples and IR pyrometers.

The results, Figure 4.3.4 (left) showed variations in the effective gas/particle temperatures for different lines of sight. Gas IR emission spectra consist primarily of $CO_2$ and $H_2O$ emission bands that make data analysis possible with the use of the latest version of the HITEMP spectral database[21]. Modelling of $H_2O$ spectral emission (1000 $cm^{-1}$ to 6000 $cm^{-1}$) for various temperature profiles and over long distances show that effective $H_2O$ emissivity and temperature depend on the temperature profile uniformity. Thus a constant temperature profile gives exactly the same emissivity (i.e. 1) and temperature. Conversely, a non-uniform temperature profile gives lower effective emissivity (<1) and temperature. The effective emissivity of $H_2O$ can be used to evaluate the uniformity of the temperature profile. Another conclusion is that low spectral resolution (from 8 $cm^{-1}$ and lower) and high sampling rate are preferable because of turbulence effects in the gas, especially at low plant loading.

In Figure 4.3.4 an overall fit by black (gas) and grey (particles) bodies are shown (based on Planck's law). The fit is based on use $H_2O$ bands and gas-free spectral ranges such as around 2600 $cm^{-1}$ and 4500 $cm^{-1}$. It can be seen that the overall emission spectrum is well described by the two fits (red and black lines) that will give effective gas and particle temperatures. The fits show that gas is quite uniform along the line of sight. Figure 4.3.4 (right) shows a comparison between effective gas and particle temperatures obtained from various line of sight measurements with plant's IR pyrometer (installed 3.5 m below the measurement location, narrow field of view). The IR pyrometer shows gas temperature variations about ± 21 °C because of gas non-homogeneity. As one can see the FTIR line of sight gas temperature measurements at 0° are in good agreement with the IR pyrometer ones taking into account the difference in instruments locations. The other observation is that the gas is colder in the -90° direction than in the +90° one, while it is in opposition for the -45° and +45° directions, although still quite uniform in temperature. This shows the complexity of large scale industrial systems

[19] Ren T, Modest M F, Fateev A, Sutton G, Zhao W, Rusu F 2019, Machine learning applied to retrieval of temperature and concentration distributions from infrared emission measurements, *Applied Energy* 252 113448

[20] Part of the selective non-catalytic reduction process employed by the plant.

[21] Rothman L S, Gordon I E, Barber R J, Dothe H, Gamache R R, Goldman A, Perevalov V, Tashkun S A, Tennyson J 2010, HITEMP, the high-temperature molecular spectroscopic database, *J. Quant. Spectrosc. Radiat. Transfer* 111 2139-2150

compared to the laboratory based ones. If the gas temperature along a line of sight is non-uniform the fits of the overall spectra will be poor and radiative heat transfer modelling tools are required in order to deduce a gas temperature profile.

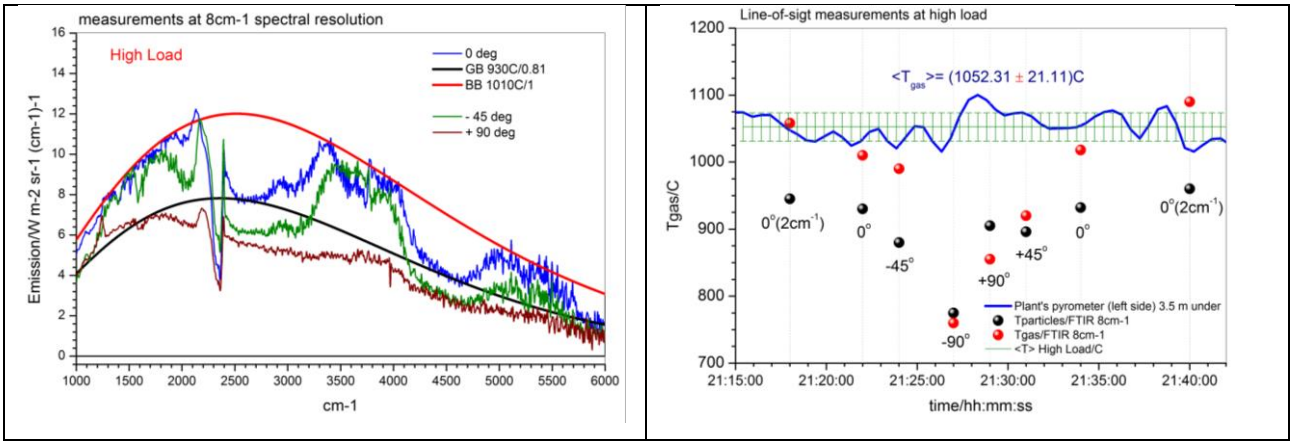


Figure 4.3.4 Left: representative emission measurements at high load operation of the plant (blue: 0°; olive -45° and wine +90° line of sight angles). Spectral resolution: 8 $cm^{-1}$. Black body (Plank's law at 1010 °C) and grey body (930 °C, emissivity 0.81) are given for the 0° case by red and black lines, respectively. Right: effective gas (red) and particle (black) temperatures at various lines of sights. Temperature measurements by the plant's pyrometer are shown by blue line. Olive: an averaged over given time window gas temperature (1052 °C) with error bars (± 21 °C).


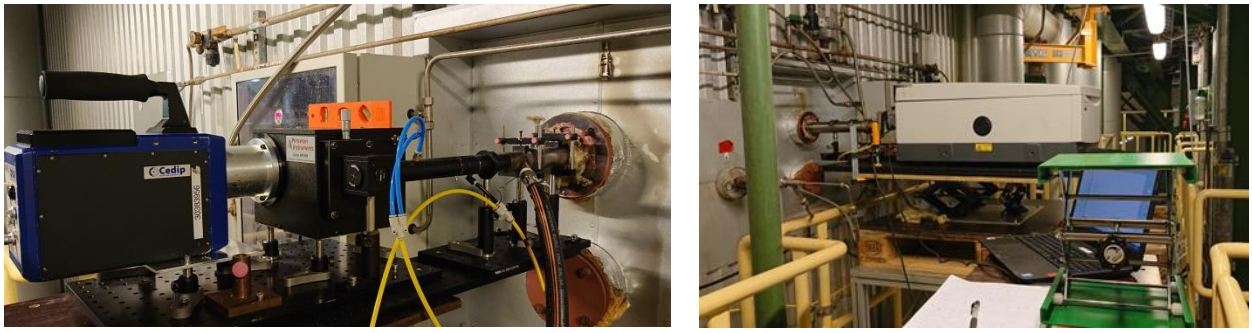

Figure 4.3.5. Top: Filborna WeT waste incineration plant. Bottom: Parallel fast IR emission measurements with IR spectrometer and CEDIP IR camera (left panel: left boiler side) and FTIR spectrometer with sweeping probe (right panel: right boiler side). Both systems are viewing the same axis.

During a service stop in the summer of 2019, B&W Vølund modified two existing access ports for cross-stack and line-of-sight measurements at the Filborna WeT plant. These ports enable simultaneous IR emission measurements with the sweeping system and cross-stack temperature and gas-composition profile mapping.

A new measurement campaign at Filborna WeT plant was completed in August 2021. Figure 4.3.5 shows simultaneous line-of-sight fast IR emission measurements with use of the FTIR spectrometer and IR grating spectrometer equipped with the CEDIP IR camera. The FTIR measurements were made at 8 $cm^{-1}$ spectral resolution and the fast scanning FTIR mode (100 kHz).

The FTIR was installed at the right access port ot the boiler while the left access port was used for other measurements (e.g. with fast IR grating spectrometer, a conventional suction pyrometer or gas sampling heated probes). The suction pyrometer (a probe containing a calibrated thermocouple with an arrangement to pull the gas around the thermocouple tip to maximise the accuracy of the gas temperature measurement) and gas sampling probes are used for local gas temperature and composition measurements across the boiler. Measurements of gas temperature with suction pyrometer are somewhat time consuming and the suction pyrometer requires thermocouple calibration – and it is prone to contamination and blocking. Use of the sight measurement approach, validated against a portable standard flame, is of great interest to the plant operators.

Figure 4.3.6 (left) shows visible images of the highly non-uniform hot gas taken an interval of 4 s apart from the right side of the boiler, and the temperature measured as a function of distance along the line of sight. The patterns are quite stable over that short period of time.

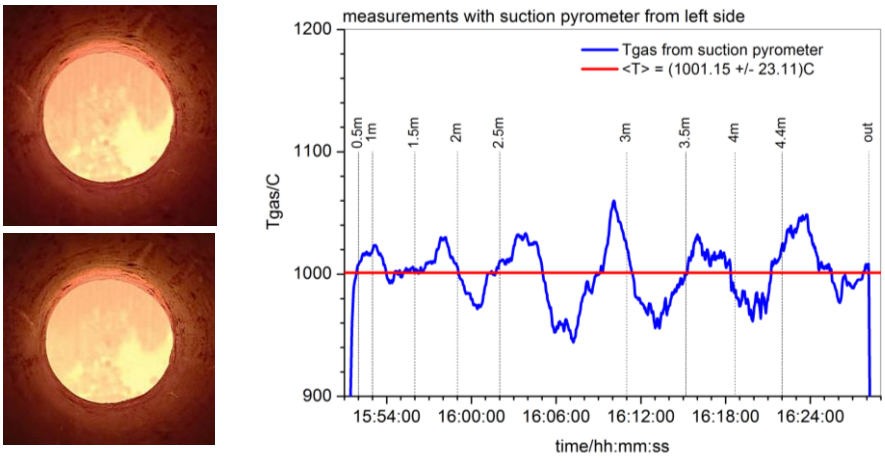


Figure 4.3.6. Left: Two visible photographs of hot gas from the right side of the boiler (FTIR spectrometer side). The two photos are taken 4 s apart. Two darker dots near the centre are access ports on the opposite side of the boiler. The gas is highly non-uniform in temperature, although there is no significant pattern change in the field of view over a duration of 4 s. Right: Gas temperature profile measurements with a suction pyrometer (from left boiler side to about the middle of the boiler) (blue) and its averaged value over a given time span (red), namely 1001.15 ± 23.11 °C.

The right panel in Figure 4.3.6 shows the gas temperature profile measurements using the suction pyrometer probe with a 0.5 m step starting from 0.5 m inside the boiler (measured from the inner boiler wall) and up to 4.4 m inside. One can see that the gas temperature varies with time at any probe position and on average it is quite uniform with an average value of 1001.15 ± 23.11 °C which lies in the optimum temperature window for the SNCR process. The maximum and minimum temperatures in that time span are about 1060 °C and 940 °C respectively. It can be expected that the temperature profile from 4.4 m and towards the right boiler wall (at 10 m) will have the same behaviour as between 0.5 m to 4.4 m. Therefore a simple approach used in the analysis of the spectra of Figure 4.3.4 can be used for effective gas and particle temperature calculations.

Emission spectra measured on a different day show different patterns, as shown in Figure 4.3.7, where two representative emission spectra are shown together with an attempt at blackbody and grey body fits. As can be seen it is impossible to perform an overall spectra fit for the gas temperature. This indicates non-uniform gas temperature profiles along the line of sight. The grey body fits can, however, be performed for both spectra, Figure 4.3.7 (left). Calculated gas emission spectra after subtraction of the grey body emission (emission from the opposite wall and particles in the gas) are about the same despite two hours' difference between the measurements, as seen in Figure 4.3.7 (right). The major difference between the spectra is due to $H_2O$ self-absorption in colder gas layers (along the line of sight) while the overall spectral shapes (defined primarily by $H_2O$ emission bands) remain the same. Because the spectra shapes depend on gas temperature and gas composition this indicates very stable operating conditions of the plant over the two hour timespan.

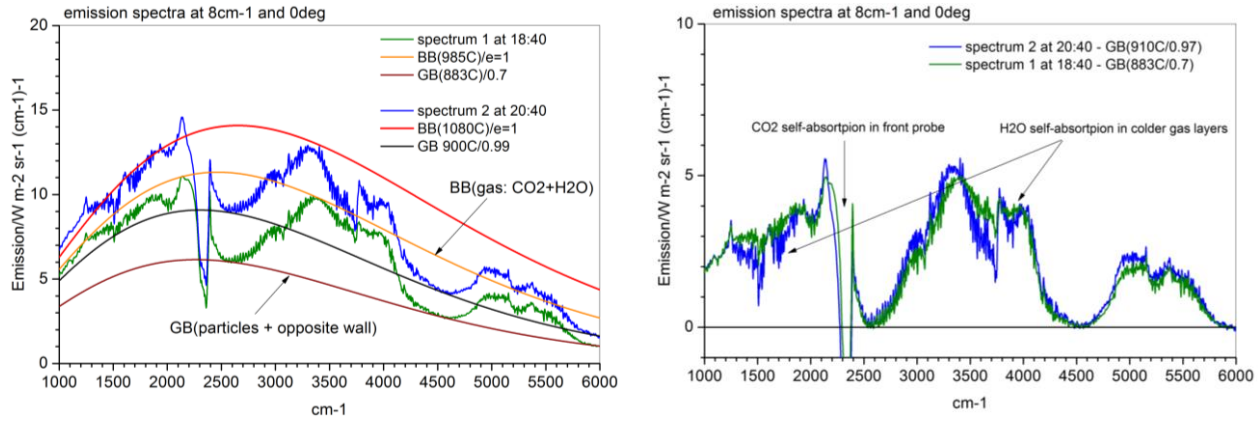


Figure 4.3.7 Left: two representative emission spectra measured at 8 $cm^{-1}$ spectral resolution (blue, olive) at different times. Black body and grey body fits are shown by red/black and orange/wine lines. Right: spectra from the right after subtraction of grey body fits. Regions affected by $CO_2$ and $H_2O$ self-absorption are marked by arrows.

The spectrum 2 from Figure 4.3.7 is shown again in Figure 4.3.8 (right) together with its modelling with use of $H_2O$ emission bands and opposite wall radiation transferred through the gas (red, radiative heat transfer calculations based on the HITEMP 2010 spectral database). Inclusion of $CO_2$ has only a minor influence on the modelling results in the wavelength ranges 1000 $cm^{-1}$ to 1120 $cm^{-1}$, 2060 $cm^{-1}$ to 2460 $cm^{-1}$, 3400 $cm^{-1}$ to 3760 $cm^{-1}$ and 4680 $cm^{-1}$ to 5160 $cm^{-1}$ where $CO_2$ bands appear. The retrieved gas temperature profile used for the spectral modelling is shown in Figure 4.3.8 (left). The gas approaches a temperature of 1300 K in the middle and shows a slightly asymmetric temperature profile towards the boiler walls. This is in opposition to the case shown in Figure 4.3.6. By a combination of retrieval results at various lines of sight it is possible to create 2D temperature plots. However, this requires a combination of fast sweeping and fast FTIR measurements and retrievals based on a machine learning approach. This will be implemented in future developments of a commercial system.

The project successfully achieved the objective with all these results.

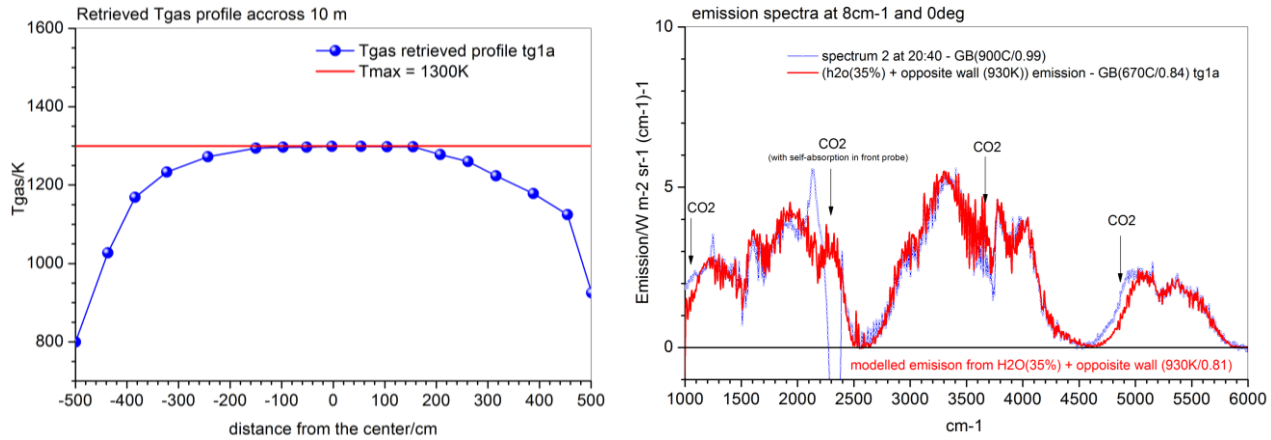


Figure 4.3.8. Left: retrieved temperature profile in 0o line of sight (blue) for the spectrum 2 (right). Right: spectrum 2 from Fig. 4.3.7 (after subtraction of grey body fit, blue) and its fit with use temperature profile (from left) and emission from opposite boiler wall (930K, emissivity 0.84) with use only $H_2O$ emission bands (red). Spectral regions with $CO_2$ contribution are marked by arrows.

### 4.4 Objective 4: Introduce traceable fibre-optic thermometry

***- by developing reliable, accurate and validated methods for demonstrating the traceability of at least two different types of fibre-optic thermometry in hostile environments. In addition, to develop novel methods for fibre-optic thermometry, validated in at least one harsh environment with a target uncertainty of better than 5 °C up to 500 °C.***

In EMPRESS 2, a suite of new fibre-optic techniques were developed with the aim of making traceable temperature measurements in harsh environments possible. Phosphor-based fibre-optic thermometry was developed using a traceably calibrated phosphor to more than 600 °C using a new type of coating for the fibre. For ionising radiation environments, a hollow-core fibre-optic thermometer was developed, which is suitable for high gamma radiation environments, as the hollow geometry renders the fibre potentially immune to the darkening effects. A distributed fibre-optic temperature sensor was developed, alongside a traceable calibration method. Its performance was investigated with a range of coatings. For high temperatures, a hybrid thermometer based on a Fibre-Bragg Grating (FBG) at the tip of the sapphire fibre and a blackbody was developed which exploits the redundancy of the two complementary measurements, and which can be traceably calibrated.

*Development of traceable phosphor-based contact thermometers to 650 °C*

The aim of this task is to develop, calibrate and test novel phosphor tipped fibre-optic thermometers up to 650 °C that are immune to electromagnetic interference. This includes field trials in suitably harsh environments to demonstrate their performance. NPL and DTI each developed a phosphor-based fibre-optic thermometer to 650 °C and cross-validated them. They then jointly established traceable calibration methods for the new fibre optic thermometers using fixed points and liquid baths from room temperature to 650 °C.

NPL have commissioned the fibre-optic thermometer calibration facility comprising two dry-block calibrators covering the temperature ranges from -45 °C to 100 °C (uncertainty 0.12 °C) and from 50 °C to 700 °C (uncertainty 1.6 °C).

NPL have selected a phosphor ($Mg_4FGeO_6$:Mn) and binder (Ceramabind 643-1) and suitable high temperature gold coated fibres have been identified. The thermometer has been built with the MFG:Mn phosphor powder encapsulated in a ceramic tube that is bonded to the cleaved end of the fibre (Figure 4.4.1). The instrumentation has a blue (420 nm) LED coupled to the fibre that excites the phosphor. A dichroic beam splitter separates the emitted radiance from the excitation and the emitted radiance is further divided into wavelength bands at 630 nm and 660 nm, again with a dichroic beam splitter. The signal at each wavelength band is detected with a new design of high sensitivity photodiodes (Hamamatsu S2387 1010) with NPL designed and built transimpedance amplifiers that have gain between 107 V/A and 109 V/A. A National Instruments USB-6356 data acquisition unit records the amplified signals. The ratio of the signals at the two wavelengths is temperature dependent and the system has been tested from -90 °C to 660 °C. Below room temperature a stirred bath was used with its temperature given by a calibrated 25 Ω standard platinum resistance thermometer and F700 resistance bridge, and above room temperature a dry block calibrator with its temperature given by a calibrated Type R thermocouple. The effect of signal excitation level, a known influencing factor, has been assessed as well as other uncertainty contributions. The target uncertainty of 5 °C at temperatures up to 500 °C was achieved.

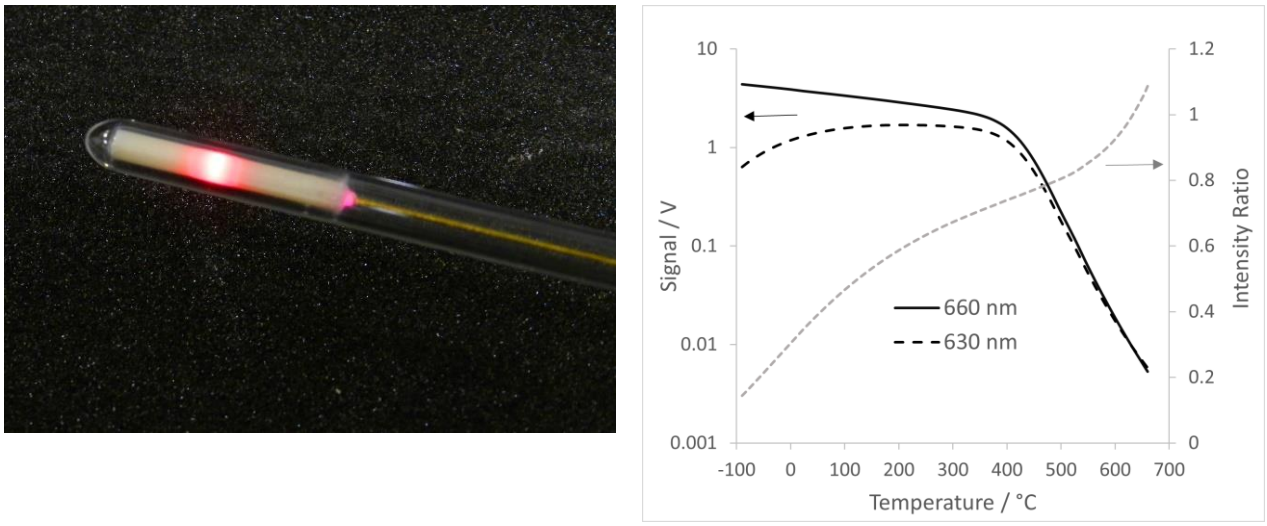


Figure 4.4.1. Left: NPL phosphor-tipped fibre-optic thermometer. Right: Phosphor intensity ratio calibration from -90 °C to 660 °C.

DTI has established the hardware and software for a fibre-optic based phosphor thermometer based on the lifetime method up to approximately 400 °C. Two separate gold-coated optical fibres are used in the thermometer, one to transmit light from the 415 nm LED to the phosphor and the other to collect light for the lifetime determination. The device was traceably calibrated and its reproducibility assessed; the reproducibility was found to be within 2 °C up to 400 °C. A model for the temperature dependence of the phosphor lifetime was developed and the calibration data was fitted to the model, yielding a practical temperature sensor with an overall measurement uncertainty of 3 °C.

*Development of novel fibre-based thermometers for harsh environments*

The aim of this task is to develop and test a novel fibre-optic based thermometer incorporating hollow core fibres. It operates over a modest temperature range (20 °C to 150 °C) but has the potential for immunity to high gamma fluxes.

UoS has investigated various types of hollow-core optical fibres (which offer higher immunity to gamma fluxes) for a phosphor-tipped fibre-optic thermometer, and have concluded that for phosphor excitation at 420 nm and emission at 660 nm, antiresonant-type fibres are the most promising options. The new design is able to deliver the excitation signal to the phosphor at the distal end and collect and guide the emitted signal back to the proximal end for analysis. Two types of anti-resonant hollow-core fibre samples, the 'tubular' and 'nested antiresonant' fibre have been fabricated and a significant effort deployed to interface them with standard optical components.

NPL has assessed these fibres for gamma radiation immunity in NPL's irradiation facility. The transmission losses at 420 nm and 630 nm were approximately 16 dB/m and 12.3 dB/m respectively. The change in transmission following an exposure of 400 Gy was less than 2 %[22]. The change in transmission ratio of two 20 nm bands at 630 nm and 661 nm (potential device specification) was less than 1 %. This demonstrates that it should be possible to operate an intensity ratio phosphor thermometer with high gamma immunity using hollow-core fibres. Additional gamma irradiation of the hollow-core fibre sample at NPL using the Cobalt 60 source was carried out. The hollow-core fibre showed robust resistance to radiation at the emission wavelength of the MFG phosphor but had not been optimised for the transmission of the excitation wavelength. However, the irradiation tests revealed that single-mode fibres optimised for solarization-free operation in the visible wavelength region had robust resistance to ionising radiation at the excitation wavelength of 450 nm. Using a combination of single-mode fibre for excitation and the hollow-core fibre for collection, UoS and NPL demonstrated a phosphor thermometer suitable for operation in harsh environments. The thermometer was characterised and showed reliable temperature measurements between 20 °C and 200 °C.

The two phosphor-tipped fibre-optic thermometers were then trialled in a very high magnetic field (NPL) and electron beam in a healthcare application (DTI) (more details in the Section 'Industrial trials and early uptake of fibre-optic thermometry').

*Distributed temperature sensors using Brillouin scattering up to 650 °C*

The aim of this task was to develop a fibre-optic distributed temperature sensor (DTS) using Brillouin scattering for use in harsh environments, and to evaluate its performance. Different coatings of aluminium and copper to suit specific applications were optically characterised to assess the Brillouin frequency shifts, ageing, and attenuation of at least two different single-mode optical fibres. The response of the two different fibre-optic coatings to a range of different temperatures up to 650 °C was also assessed.

The work here focused on Brillouin scattering, which is a process through which an incident photon interacts with a crystalline lattice to produce a phonon, losing or gaining energy in the process (the so-called Stokes process).

The photon frequency shift is detected by the comparison of two beams, one of them used as a reference, and the other interacting with the optical fibre. These two beams are generated in a unique source and then the radiation is divided into two. The distributed sensing is achieved by analysing the time of flight of the pump pulse. The photons' frequency shift depends on the fibre atoms' vibration frequency, which depends on the fibre refractive index and therefore the fibre temperature.

[22] 1 Gy corresponds to 1 Joule of energy deposited in 1 kg of material; to put it in context, a dose of 10 Gy is fatal within a few hours.

The Brillouin frequency shift was measured with the equipment designed and built by the Universidad Alcalá de Henares (Spain) and was based on the Brillouin Optical Time-Domain Analysis (BOTDA) technique[23], achieving a resolution of about 1 metre and a maximum spatial range of about 30 km.

CEM performed the calibration of at least three of the differently coated fibre-optic DTS up to 650 °C, by immersing the fibres in a highly uniform tube furnace with the traceable reference temperature provided by an Au/Pt thermocouple at a Pt100. The fibres were coiled, without torsion, and kept horizontal in the furnace to avoid any spurious temperature gradients.

Tests of the distributed fibre-optic sensor were planned in a stainless steel manufacturing process at CEM, but ultimately these were not possible due to restrictions associated with the global Covid-19 pandemic.

*Hybrid fibre-optic based high temperature sensor to 1500 °C*

The aim of this task is to develop novel fibre-optic based temperature sensors that will be capable of operation up to 1500 °C and to demonstrate that, with field trials in extreme environments. Specifically, Fibre-Bragg Grating (FBG) thermometers offer great potential for high temperature applications. However, silica-based fibres are currently limited to around 1000 °C and they are prone to grating degradation at higher temperatures. This task will develop Bragg and blackbody cavity fibre-optic sensors based on sapphire fibres with the aim of combining them in a single hybrid sensor. By doing this, confidence in the measurement is greatly improved as the measurement uncertainty is expected to be halved.

IPHT were responsible for developing optoelectronics and signal processing instrumentation and preparing sapphire FBGs in test fibres. PTB developed signal processing algorithms for the temperature dependence of the asymmetric resonance peak of the FBGs in relation to the stability, repeatability and resolution of the measurements. JV advised on the compatibility of the sapphire FBG with the blackbody part of the sensor.

IPHT and PTB established the design of the sapphire FBG thermometer. PTB designed and assembled a measurement setup for the high resolution spectral analysis of FBGs, which is based on a tuneable laser source. The software integration of all components is complete, and the characterisation of the thermometers provided by IPHT is underway.

IPHT have developed inscribed Fibre Bragg gratings with an operating wavelength of about 1540 nm in several fibres with a length of more than 80 cm, so that the probe will fit into the calibration furnaces at PTB. IPHT packaged sapphire fibres with protection tubes and conventional optical fibres, and in the first series of measurements no ageing effects were observed. Different signal processing algorithms for the asymmetric peak detection were investigated on a prototype device. An ITS-90 traceable calibration of a FBG thermometer based on sapphire fibre was performed up to 1500 °C at PTB.

IPHT have also established a test facility to provide temperature environments up to 1500 °C. The effect of self-radiation on the blackbody radiation was investigated. IPHT recorded spectrally resolved data in immersion tests in a furnace. Analysis performed by JV and IPHT showed a substantial self-radiation issue, and a model was developed to help mitigate against this.

PTB advanced the laser-based setup with SI traceable gas cells to provide a wavelength reference. Several datasets on the spectral reflection coefficient at different temperatures have been acquired, as measured using the tuneable diode laser setup. The data shows interference effects from the multimode transmission in the sapphire fibre. While the interference patterns are stable and repeatable, they pose a signal processing challenge which limits the resolution of the FBG thermometer. The device was trialled in a very harsh silicon processing environment (described below in the section ‘Industrial trials and early uptake of fibre-optic thermometry’), and additionally inside an industrial-grade drawing tower for fused silica fibres in which an induction furnace is used to heat the material up to 1700 °C during the tests.

Industrial trials and early uptake of fibre-optic thermometry

*Control of electron beams for dose planning in radiotherapy*

Field trials were performed by DTI at Aalborg University Hospital (AUH) to test the robustness of the $Mg_4FGeO_6$:Mn thermographic phosphor based optical fibre thermometer under harsh environmental conditions due to exposure of charged particles (electrons). A temperature sensor which is immune to charged particles will enable industry, science and health organisations to conduct reliable temperature measurements

[23] R. Ruiz-Lombera, I. Laarossi, J. Mirapeix, M.A. Quintela, J.M. Lopez-Higuera, High-temperature distributed sensor system via BOTDA and multimode gold-coated fiber, Proceedings of the SPIE, Volume 9916, id. 991632 4 pp. (2016)

under the harsh conditions of charged electron bombardment, e.g. in cancer therapy, where the temperature is a critical parameter to ensure an optimal individual treatment of patients and correct dose planning.

The sensor used is composed of two separate aluminium coated multimode fibres, which have a stainless steel flexible protection tube and are terminated by an SMA connector at one end. At the other end, the two fibres are inserted into a double-bore, open-end ceramic tube, which again is inserted into a single-bore closed-end ceramic tube with MFG powder at the tip (Figure 4.4.2).

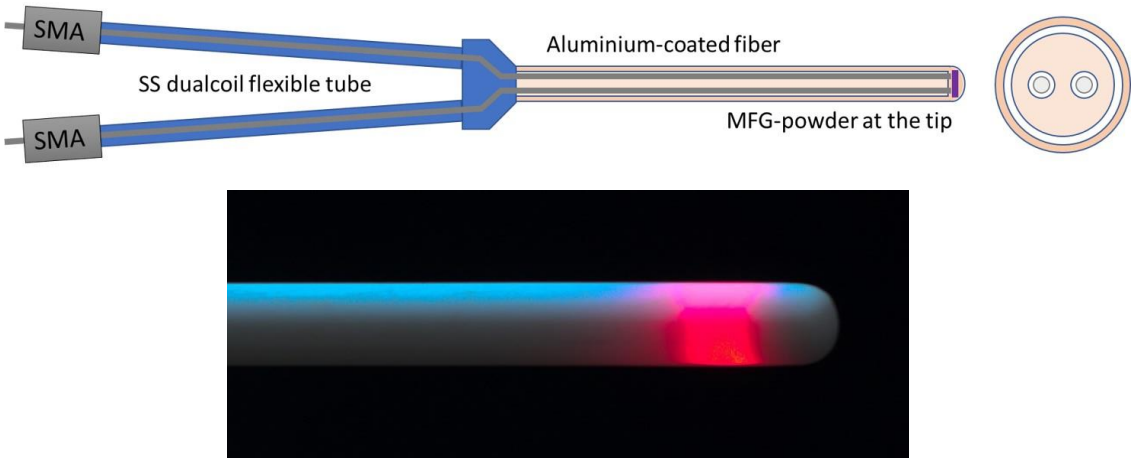


Figure 4.4.2. Top: Phosphor thermometer sensor construction. Bottom: the light emitted from the phosphor powder can be seen through the outer ceramic tube, and the intensity of the light can be optimised to maximise the signal to noise ratio of the sensor.

The purpose of the optical light detection and signal processing system is to process the light emitted from the phosphor and calculate the corresponding temperature. The setup is illustrated in Figure 4.4.3. The LED is controlled by a fast LED driver and the blue electrical signal in the graph of Figure 4.4.3 is transmitted to the LED, which will quickly switch on and off and emit relatively sharp light pulses of 50 ms duration and at a frequency of 10 Hz. The light pulse is then transmitted to the MFG powder at the sensor tip and as the light arrives the phosphor will start to emit light at wavelengths between 600 nm and 700 nm. The emission of light from the phosphor will build up until the phosphor is fully saturated as shown by the red curve of the graph in Figure 4.4.3. To minimise the noise from the surrounding light, a short pass (cut-off wavelength 750 nm) and a long pass (cut-off wavelength 650 nm) was installed in the light beam before the light was transmitted onto a silicon avalanche photo diode (Si APD). This type of detector was chosen to optimise the detection of light and thus the temperature measurement at high temperatures, where the signal strength and its lifetime gradually reduces. The signal is captured in a fast, high-resolution oscilloscope (picoScope 5444D).

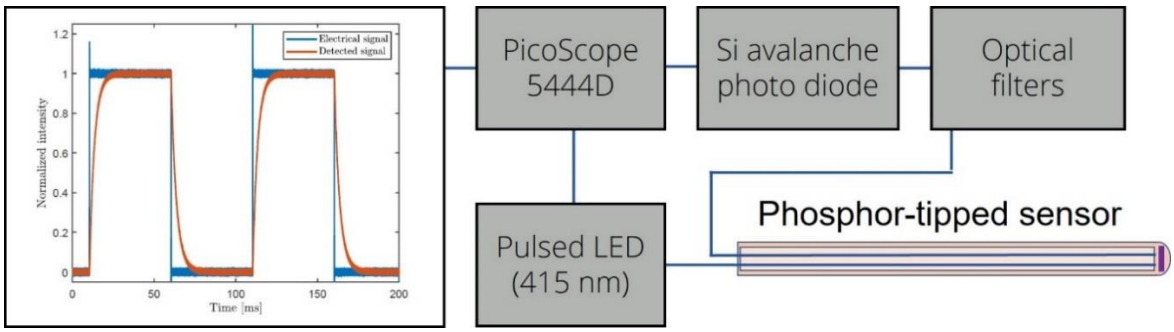


Figure 4.4.3. Setup of the optical light detection and signal processing system. 415 nm pulsed light from the LED is transmitted via the optical fibre to the tip of the sensor, where the phosphor is excited to emit light in the wavelength range from 600 nm to 700 nm. The emitted light is transmitted via the other fibre to the detector, and the lifetime is estimated to determine the temperature.

All the hardware is operated automatically in a LabVIEW program, which also automatically characterises the signal and performs a correction based on the traceable calibration performed prior to use. The phosphor

decay lifetime is assessed with a frequency of about 0.5 Hz, so the temperature can be measured at approximately this rate.

The thermometer was traceably calibrated using an Ametek RTC-700 dry-block calibrator with digital load compensation to minimise the temperature gradient in the insert of the dry-block. In an automatic calibration setup, the temperature of the calibrator is controlled automatically in steps of 20 °C, and the calibrator is allowed to stabilise before five consecutive lifetime spectra are acquired. The ITS-90 traceable temperature is found from the Pt-100 reference sensor inserted into the dry-block together with the phosphor thermometer, as shown in Figure 4.4.4.

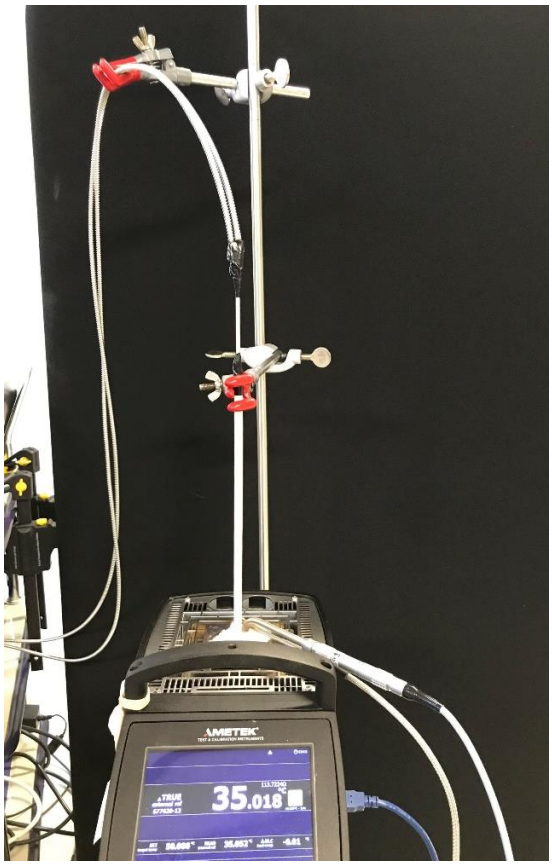


Figure 4.4.4. Setup for calibration of the phosphor thermometer using a dry-block calibrator.

To examine whether the phosphor thermometer is immune to a continuous flux of charged particles, a field trial was conducted in which the sensor was exposed to a well characterised dose of 9 MeV and 20 MeV electrons, respectively, from a cancer treatment apparatus at Aalborg University Hospital. Using a solid water phantom as build up material, the equipment was positioned at the water equivalence depth[24] for each electron energy. The setup is shown in Figure 4.4.5. The sensor was exposed to 9 MeV and 20 MeV electrons, respectively, from the top. The dose is controlled with water plates on top of the sensor.

After establishing a stable temperature, the electron beam was switched on and the sensor exposed to the beam for five minutes. The beam was switched off for about 1.5 minutes, then switched on again. Figure 4.4.6 shows the temperature measurement during the beam exposure; it can be seen that the beam has no effect on the temperature reading.

[24] INTERNATIONAL ATOMIC ENERGY AGENCY, Absorbed Dose Determination in External Beam Radiotherapy, Technical Reports Series No. 398, 2000

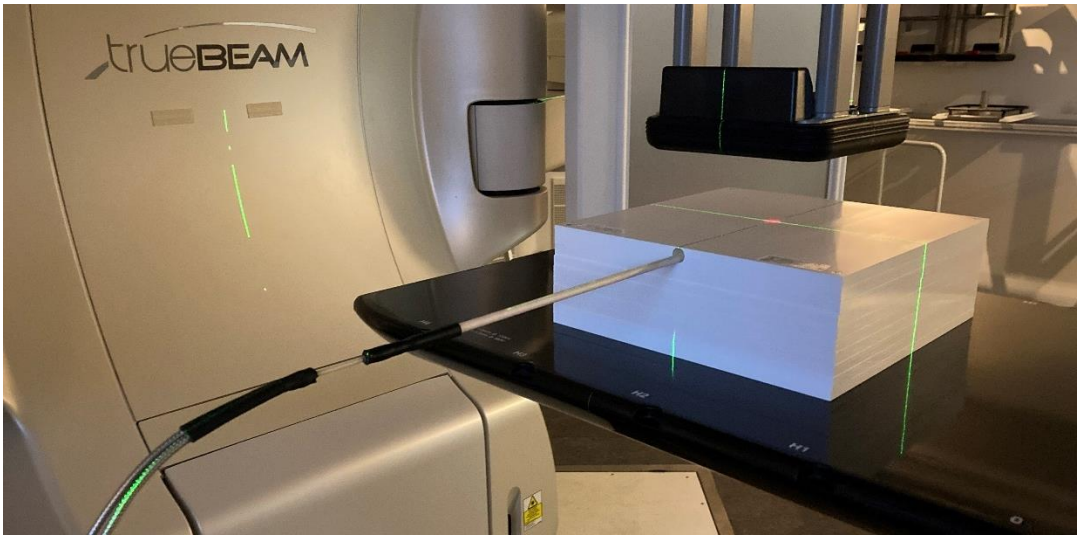


Figure 4.4.5. Setup at AUH to expose the phosphor thermometer to 9 MeV and 20 MeV electrons.

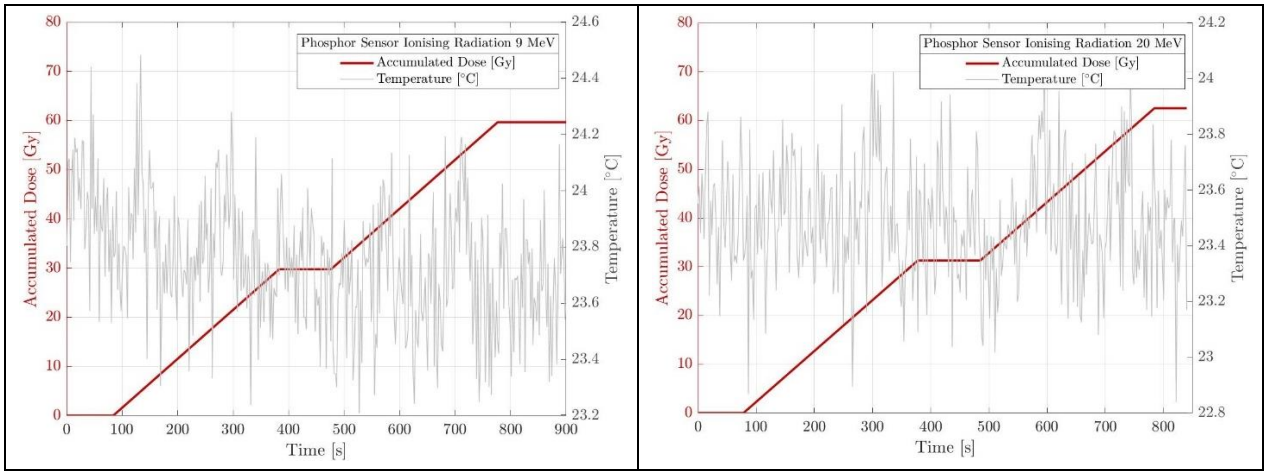


Figure 4.4.6. Temperature indicated by the thermometer during radiation exposure (gray line, left axis) and accumulated radiation dose (red line, right axis). Left and right panels indicate two separate measurements.

The thermometer was traceably calibrated before exposure to the electron beam exposure, and again afterwards, as shown in Figure 4.4.7. It appears that the calibration has shifted following the exposure to charged particles, but it cannot be stated definitively whether this is significant. Nonetheless, it can be stated that the reproducibility of the temperature measurements are within the target of ±3 °C.

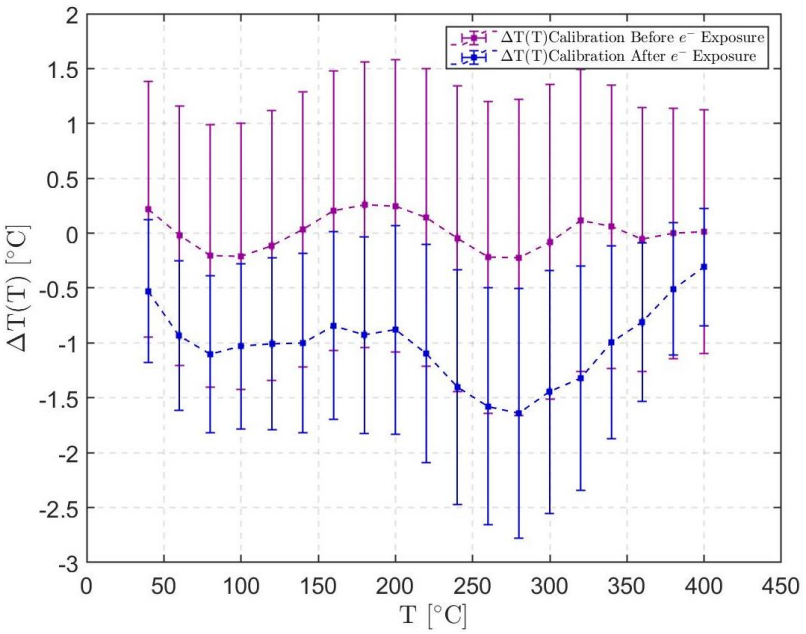


Figure 4.4.7. Calibration of the phosphor thermometer (expressed as a measurement error) before and after exposure to the electron beam.

*High magnetic fields*

Tests were carried out at NPL comparing phosphor tipped fibre-optic thermometer, a Type R thermocouple and a Pt100 resistance thermometer. The thermocouple was made at NPL from 0.5 mm diameter nominally 99.99 % wire in twin bore alumina. It had a bare junction in a silica tube – a metal sheath which might have shielded the junction would be unsuitable in a magnetic field of more than 2 T. The Pt100 was an R-series from IST, 4-wire 2.8 mm diameter and 13 mm long.

Measurements were made at the NPL Electronic & Magnetic Materials Group, using a Bruker electromagnet capable of generating up to 3 T at the centre of the gap. Traceability for the magnetic field measurements is obtained via frequency using a nuclear magnetic resonance technique. Tests on smaller AC fields (to 20 mT) had shown that heating in the magnet coils and variation in laboratory temperature between tests would mask any small effects. Therefore, the three probes were mounted together between the poles of the Bruker electromagnet as shown in Figure 4.4.8.

The electromagnet was cycled from 0 T to 2.3 T and back five times. It was apparent that there was a steady increase in ambient temperature during this time. To remove this drift a linear fit to each dataset was used as a baseline, and measurements were normalised to this reference. Figure 4.4.9 shows the change in measured temperature of the type-R thermocouple and phosphor thermometer with the changing magnetic field. As the field increases and decreases the measured temperature likewise increases and decreases by 0.6 °C. During zero field conditions the thermocouple reads the same as the phosphor thermometer. The dominant effect is electrically driven, not thermal, since when the magnetic field is reduced the thermocouple reads lower temperatures than the baseline corresponding to the temperatures measured at zero field.

Figure 4.4.10 shows the equivalent situation with the Pt100 resistance thermometer. In this case the Pt100 reads high when the magnetic field is on, and possibly the phosphor thermometer does as well. It is noticeable that there is an overall change in the base-line from start to end, albeit only a few milli-Kelvin, but it does appear that something is warming up, possibly one of the sensors, when the field is on and that both the resistance and the phosphor thermometers are picking this up.

In terms of absolute temperature measurement and including calibration uncertainty, overall, the Pt100 was 20.33 °C ± 0.04 °C and the phosphor thermometer was 21.51 °C ± 1.56 °C. These agree within the uncertainties.


Figure 4.4.8. The three probes – phosphor, thermocouple and resistance – mounted between the poles of the magnet.

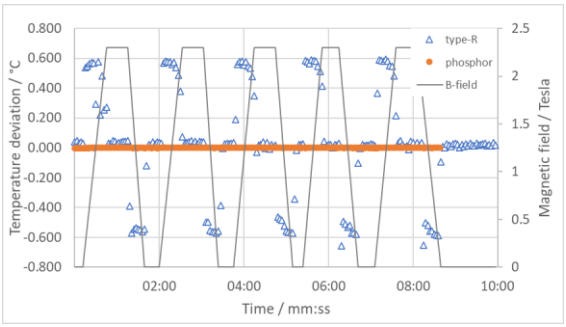


Figure 4.4.9: Deviation of the Type R thermocouple and phosphor thermometer from base-line temperature as the magnetic field alternates between zero and 2.3 Tesla.

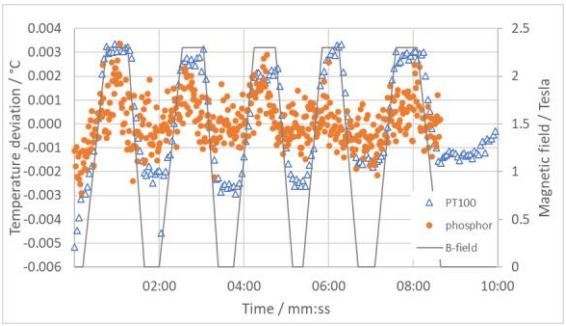


Figure 4.4.10: Deviation of the Pt100 resistance thermometer and phosphor thermometer from base-line temperature as the magnetic field alternates between zero and 2.3 Tesla.

*Silicon processing for photovoltaic solar panel manufacture*

Temperature measurement up to 1500 °C is very challenging and often left to thermocouples or non-contact methods e.g. thermal imaging or pyrometers. However, in some cases these are unsuitable, and the advantages of a fibre-optic based thermometer are needed. To address this, a hybrid thermometer was constructed by IPHT, PTB and JV based on a Fibre-Bragg Grating (FBG). The FBG consists of a regular array written with femtosecond laser pulses into the sapphire fibre, which changes its reflection spectrum with temperature; by measuring this the temperature can be determined. The fibre also provides access to the thermal Planck radiation of the probe, which can be analysed with the same set-up as the FBG spectrum and enables a hybrid temperature determination.

Typical silica-based fibres are currently limited to around 1000 °C. FBGs in sapphire fibres have shown great potential, but they are currently limited in their measurement precision due to the complex multi-mode reflection peak. The challenge here was to develop FBG fibre-optic sensors based on sapphire fibres with the aim of combining FBG and the Planck radiation signal in a single hybrid sensor. By doing this, confidence in the measurement can be greatly improved as the redundancy of the two methods can be exploited.

To demonstrate its performance, a triple thermometer was constructed, consisting of a sapphire fibre for the hybrid FBG/Planck signal and a thermocouple in the same sleeve. The 80 cm long probe was installed in cooperation with Elkem in a silicon melting facility at REC Solar, a photovoltaic solar panel manufacturer in Norway, operating up to 1575 °C (shown in Figure 4.4.11), where thermometry is extremely difficult with thermocouples due to the disastrous effect of silicon on the precious metal thermoelements. The first results are promising, with the triple sensor in the process at around 1414 °C (the melting temperature of pure silicon) showing good consistency between the three signals: 1417.5 °C was indicated by the thermocouple, while the FBG thermometer indicated 1416.3 °C and the Planck signal was in agreement within about ±5 °C. After several weeks in the industrial process with 300 hours above 1400 °C, the sensor was re-calibrated at PTB, where it was confirmed that the FBG signal does not drift within the measurement uncertainty.

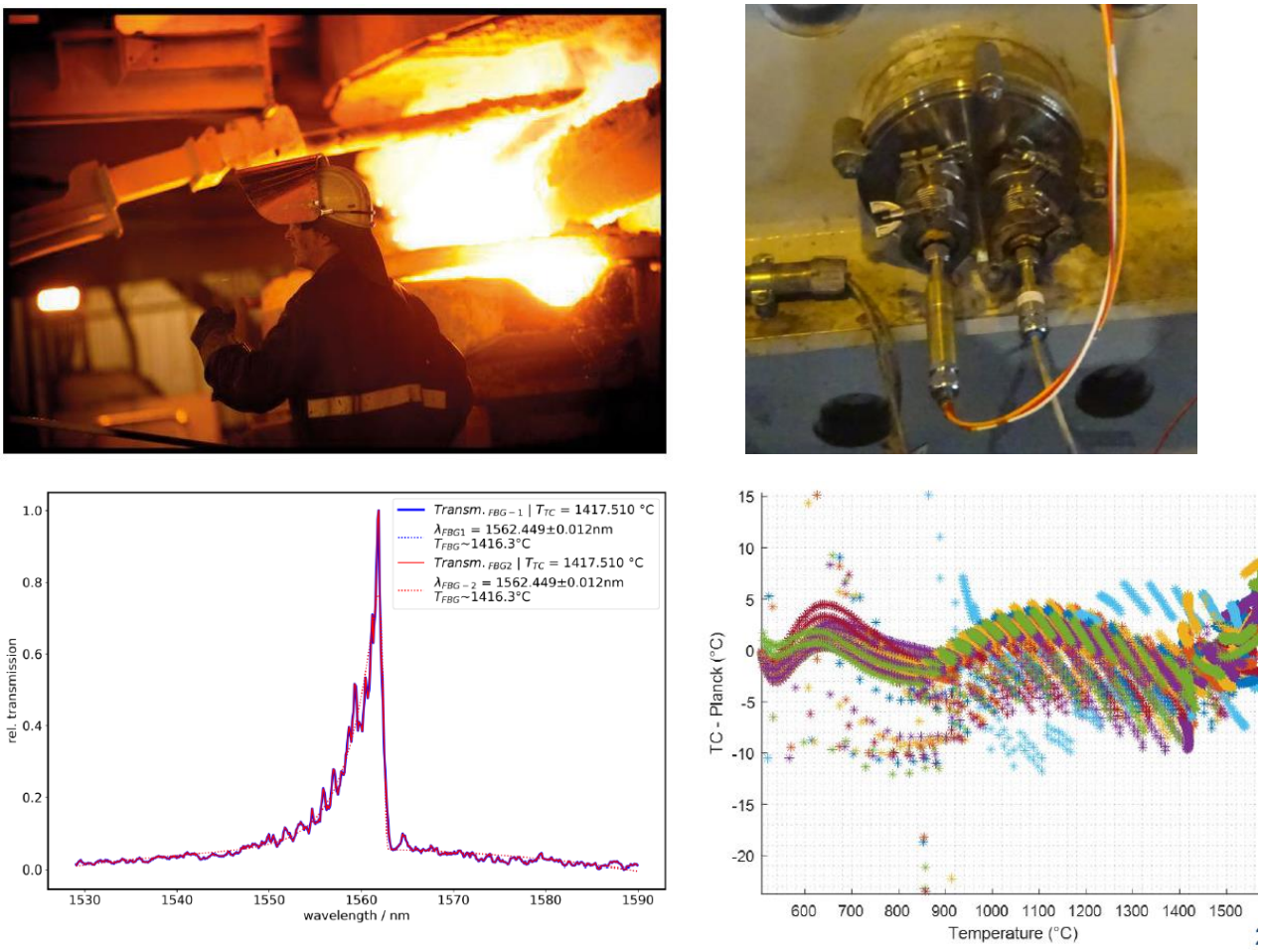


Figure 4.4.11. Top left: Silicon processing environment. Top right: Hybrid FBG/BB sensor head and thermocouple sensor head emerging from the silicon processing facility. Bottom left: Relative transmission as a function of wavelength, showing the consistency between two consecutive measurements, and the difference between the FBG and thermocouple temperature indications. Bottom right: Differences between Planck derived temperatures and the temperature indicated by the thermocouple.

The hybrid thermometer was calibrated before and after the tests at REC Solar. The final calibration yielded drift at the Al and Cu ITS-90 fixed points as follows (uncertainties $k$ = 2 corresponding to 95 % confidence):

| Fixed point | Drift of thermocouple | Drift of FBG |
|---|---|---|
| Al (660.323 °C) | 0.2 K ± 1.2 K | 0.7 K ± 2.0 K |
| Cu (1084.62 °C) | 0.2 K ± 2.1 K | 0.5 K ± 1.7 K |

The only real problem was that the absolute calibration of the FBG was impeded by instability of the optical modes, so the uncertainty of about 2 K was achieved by good averaging of the modes in the laboratory. Unfortunately, this was not possible for the on-site measurements, so that the uncertainties during the process measurements are about 10 K to 14 K. On the other hand, the FBG measurements expressed as being relative to the thermocouple should be significantly more reliable.

The project successfully achieved the objective with all these results.

# 5 Impact

The project was industry-focused with the outputs being trialled in-process during the project's lifetime. Of particular note is the input to the discussions of the IEC committee responsible for thermocouple standard IEC 60751, input to the ASTM committee responsible for thermocouple standard E20, presentation to the NADCAP Heat Treating Task Group and SAE AMS AMEC aerospace committee meeting, input to three CCT guides, presentations at 25 international conferences on combustion thermometry, phosphor thermometry, spacecraft testing, thermodynamic modelling, thermal modelling, thermal imaging, nuclear decommissioning and measurement and control respectively. A Euramet summer school was held by partners, as well as a training course for university postgraduates; in total 16 training events were held. The EMPRESS 2 stakeholder community currently numbers 148, and a stakeholder community workshop was held by the consortium which attracted 121 delegates from across the globe. Two PhD students performed work as part of the project. 14 Open Access publications are now available and represent Technical reports, Articles in peer-reviewed journals and a Good Practice Guide. 50 other dissemination activities included trade journal articles, and workshops.

*Impact on industrial and other user communities*

The direct impact on partners will be very significant. The introduction of in-situ traceability to ITS-90 is embedded in all of the tasks of the project and this will ensure better consistency across the range of processes impacted. The longer term impact on industry will be wider. Improved temperature measurement will result in tighter process control leading to better, more consistent products which in turn enhances competitiveness. Examples of early impact include better characterisation of brake pad temperatures for automotive development applications, improved marine welding with reduced wastage and stronger end products, improved heat treatment of aerospace parts, lower uncertainty calibrations and thermocouples available from NMIs, new products for flame imaging instrumentation manufacturers, improved waste incineration facilities, new products for fibre optic thermometry manufacturers including traceability, improved characterisation of large scale industrial furnaces, more efficient large scale silicon processes, and more efficient large scale steel manufacturing processes. Early impact includes trials of **phosphor thermometry** in electro-thermal mechanical testing, photovoltaic device development, nuclear decommissioning and waste storage, marine manufacturing (welding pre- and post-heat treatment and annealing), temperature monitoring on forging tools, on-line and off-line temperature monitoring and control in forming, forging and heat treatment, and automotive braking system development. **Thermocouple thermometry** was demonstrated in quartz glass manufacturing, steel production for railways, float glass manufacturing, and industrial furnace and refractory insulation manufacturing. **Combustion thermometry** was demonstrated in the development of a low-cost thermal imaging system and in a commercial waste incineration process. **Fibre-optic thermometry** was demonstrated in the control of electron beams for dose planning in radiotherapy, high magnetic fields, and silicon processing for photovoltaic solar panel manufacture.

*Impact on the metrology and scientific communities*

The consortium has representation on the Task Group on Guides on Thermometry of the BIPM Consultative Committee for Thermometry (CCT) which is responsible for promoting good thermometry practice and traceability to the SI by preparing and publishing guides on thermometry, with an emphasis on secondary thermometry, i.e. the subject of this project. The consortium will ensure that CCT members are made aware

of the project's outputs. The consortium also has representation on the EURAMET Technical Committee on Thermometry (TC-T), including the Chair, and has been ensuring that the project's outputs are widely disseminated via EURAMET TC-T activities including the Euramet Summer School on Metrology, and presentations at the annual meeting and an associated workshop on the mise-en-pratique for the redefinition of the kelvin; a Euramet guide on thermocouple calibrations which span out of this work was also published. A member of the consortium chairs the Spanish National Accreditation Body, Entidad Nacional de Acreditación (ENAC) subcommittee for Temperature and Humidity (ENAC SCTC11). Standards bodies in Germany, Italy and Turkey are also linked to the project. In addition, a partner was president of the Institute of Measurement and Control (InstMC) during the project's lifetime, greatly facilitating the dissemination of the project's outputs.

There are a number of smaller NMIs in the consortium and their participation in this project contributed substantially to capacity building, particularly in the area of thermocouple calibration and the facilities and skills required for contributing to reference function determination.

*Impact on relevant standards*

This project will have a significant impact by enabling industries to ensure a greater level of compliance with relevant standards. This was achieved through influencing committees including IEC TC 65/SC 65B/WG5 (thermocouple standards); ASTM (thermocouple standards); Nadcap (National Aerospace and Defence Contractors Accreditation Program) and SAE (specific industry-wide aerospace heat treatment standards – a presentation has been given at one of their meetings); Consultative Committee for Thermometry (wide ranging areas of interest – some partners are represented on the new working group associated with photonic thermometry, i.e. fibre-optic thermometry); EURAMET Technical Committee on Thermometry (TC-T, wide ranging areas of interest, outlined in the metrology section above, who have been given regular updates by the consortium); InstMC – Standards Policy Panel (promotion of excellence in instrumentation and control); IoP ISAT committee (promotion of new developments in sensing). Specific standards that were targeted are IEC 61515 (MI thermocouple cable manufacturing – some partners were represented at the last meetings of the IEC to discuss aspects of standardisation for the new double-walled thermocouples being studied in this project), ASTM E20 (MI thermocouple cable manufacturing; some partners were represented at a meeting to input into the E20 standard revision), IEC 62460 (Non letter designated thermocouple emf versus temperature relationship) and AMS 2750E (Aerospace heat treatment; some partners were represented at a meeting in 2018 to describe the project to aerospace heat treatment prime suppliers).

*Longer-term economic, social and environmental impacts*

In regional terms, the EU is the world's largest exporter of manufactured goods. However, high energy prices have increased the economic importance of energy as an input in the production process. European firms have made great progress in improving efficiency, but this has not been enough to compensate for the increase in energy prices. Furthermore, there is growing evidence that the evolution of expertise in energy efficient processes, technologies and services means that this expertise itself can be exported, thus providing European business with a competitive edge.

The present project will assist in progressing towards these goals by demonstrating new and more accurate temperature measurement techniques to major manufacturers, such as Rolls-Royce, enabling them to better understand their processes and energy usage.

# 6 List of publications


1. The NPL portable standard flame: Operating instructions, NPL Report ENG 69, ISSN 1754-2987 http://eprintspublications.npl.co.uk/8259/
2. An investigation into a calibration scheme for a light pipe based temperature probe, Åge Andreas Falnes Olsen, Helge Mathisen, Sigurd Simonsen, 2018 Meas. Sci. Technol. 29 115004. Highlight: selected as one of the 2018 Highlights of Measurement Science and Technology https://iopscience.iop.org/article/10.1088/1361-6501/aade6f
3. Calibration of thermocouples: EURAMET Calibration Guide No. 8 Version 3.0, J.V. Pearce, N. Arifovic, J. Bojkovski, F. Edler, M. de Groot, C. Garcia Izquierdo, M. Kalemci, R. Strnad https://www.euramet.org/publications-media-centre/calibration-guidelines/
4. Validation of emission spectroscopy gas temperature measurements using a standard flame traceable to the International Temperature Scale of 1990 (ITS-90), G. Sutton, A. Fateev, Miguel A. Rodriguez-Conejo,

Juan Melendez, Guillermo Guarzino, Int. J. Thermophys. 40 99 (2019) https://doi.org/10.1007/s10765-019-2557-6

5. A validated physical model of the thermoelectric drift of Pt-Rh thermocouples above 1200 °C, J.V. Pearce, Metrologia 57 025009 (2020) https://doi.org/10.1088/1681-7575/ab71b3
6. Design, construction and calibration of a novel phosphor-based fibre-optic thermometer from 0 °C to 650 °C, D. Lowe, G. Sutton, A. Sposito, G. Machin, J. Pearce, Measurement Science and Technology 32 094004 https://doi.org/10.1088/1361-6501/abee53
7. Mass Loss of Platinum-Rhodium Thermocouple Wires at 1324 °C, S. Uthayakumaar, S. Davidson, J. Pearce, Johnson Matthey Technology Review, Volume 65, Number 4, 1 October 2021, pp. 568-573(6) https://doi.org/10.1595/205651321X16183288904988
8. Some Predictions of a Validated Physical Model of Pt-Rh Thermocouple Drift Above 1200 °C, J.V. Pearce, Metrologia 58 035011 (2021) https://doi.org/10.1088/1681-7575/abeb80
9. Mapping of temperature and CO2 column density in a standard flame by multispectral imaging, J. Meléndez, J. Talavante, G. Guarnizo, F. López, Proceedings Volume 11743, Thermosense: Thermal Infrared Applications XLIII; 117430V (2021) https://doi.org/10.1117/12.2585805
10. Pt-40%Rh versus Pt-6%Rh thermocouples: an emf-temperature reference function for the temperature range 0 °C to 1769 °C, F. Edler, J. Bojkovski, C.G. Izquierdo, M.J. Martin, D. Tucker, N. Arifovic, S.L. Andersen, L. Sindelarova, V. Zuzek, International Journal of Thermophysics Volume 42, Article number 150 (2021) https://doi.org/10.1007/s10765-021-02895-w
11. Miniature iron-carbon eutectic point crucible for the calibration of thermometers, V. Žužek and J. Bojkovski, Measurement Volume 181, August 2021, 109619 https://doi.org/10.1016/j.measurement.2021.109619
12. Thermoelektrische Eigenschaften von Pt-40%Rh/Pt-6%Rh Thermoelementen, Frank Edler and Petra Ederer, tm - Technisches Messen, (2021) https://doi.org/10.1515/teme-2021-0042
13. Correlation between insulation resistance and temperature measurement error in Type K and Type N mineral insulated, metal sheathed thermocouples, Pearce, J., Tucker, D., Izquierdo, C.G. et al., Int J Thermophys, (2022) https://doi.org/10.1007/s10765-021-02967-x
14. Multispectral Mid-Infrared Camera System for Accurate Stand-Off Temperature and Column Density Measurements on Flames, Meléndez, J.; Guarnizo, G., Sensors, (2021), https://doi.org/10.3390/s21248395

This list is also available here: https://www.euramet.org/repository/research-publications-repository-link/